Atmos. Chem. Phys. Discuss., 8, 21313–21381, 2008
www.atmos-chem-phys-discuss.net/8/21313/2008/

Atmospheric Chemistry and Physics Discussions

This discussion paper is/has been under review for the journal *Atmospheric Chemistry and Physics (ACP)*. Please refer to the corresponding final paper in *ACP* if available.

Single particle characterization using a light scattering module coupled to a time-of-flight aerosol mass spectrometer

E. S. Cross[1], T. B. Onasch[1,2], M. Canagaratna[2], J. T. Jayne[2], J. Kimmel[2,3], X.-Y. Yu[4], M. L. Alexander[4], D. R. Worsnop[2], and P. Davidovits[1]

[1]Chemistry Department, Boston College, Chestnut Hill, MA, USA
[2]Center for Aerosol and Cloud Chemistry, Aerodyne Research Inc., Billerica, MA, USA
[3]CIRES University of Colorado, Boulder, CO, USA
[4]Pacific Northwest National Laboratory, Richland, WA, USA

Received: 22 October 2008 – Accepted: 1 November 2008 – Published: 23 December 2008

Correspondence to: E. S. Cross (crosse@bc.edu)

Published by Copernicus Publications on behalf of the European Geosciences Union.

Abstract

We present the first single particle results obtained using an Aerodyne time-of-flight aerosol mass spectrometer coupled with a light scattering module (LS-ToF-AMS). The instrument was deployed at the T1 ground site approximately 40 km northeast of the Mexico City Metropolitan Area (MCMA) as part of the MILAGRO field study in March of 2006. The instrument was operated as a standard AMS from 12–30 March, acquiring average chemical composition and size distributions for the ambient aerosol, and in single particle mode from 27–30 March. Over a 75-h sampling period, 12 853 single particle mass spectra were optically triggered, saved, and analyzed. The correlated optical and chemical detection allowed detailed examination of single particle collection and quantification within the LS-ToF-AMS. The single particle data enabled the mixing states of the ambient aerosol to be characterized within the context of the size-resolved ensemble chemical information.

The particulate mixing states were examined as a function of sampling time and most of the particles were found to be internal mixtures containing many of the organic and inorganic species identified in the ensemble analysis. The single particle mass spectra were deconvolved, using techniques developed for ensemble AMS data analysis, into HOA, OOA, NH_4NO_3, $(NH_4)_2SO_4$, and NH_4Cl fractions. Average single particle mass and chemistry measurements are shown to be in agreement with ensemble MS and PTOF measurements. While a significant fraction of ambient particles were internal mixtures of varying degrees, single particle measurements of chemical composition allowed the identification of time periods during which the ambient ensemble was externally mixed. In some cases the chemical composition of the particles suggested a likely source. Throughout the full sampling period, the ambient ensemble was an external mixture of combustion-generated HOA particles from local sources (e.g. traffic), with number concentrations peaking during morning rush hour (04:00–08:00 LT) each day, and more processed particles of mixed composition from nonspecific sources. From 09:00–12:00 LT all particles within the ambient ensemble, including the locally pro-

ACPD

8, 21313–21381, 2008

duced HOA particles, became coated with NH_4NO_3 due to photochemical production of HNO_3. The number concentration of externally mixed HOA particles remained low during daylight hours. Throughout the afternoon the OOA component dominated the organic fraction of the single particles, likely due to secondary organic aerosol formation and condensation. Single particle mass fractions of $(NH_4)_2SO_4$ were lowest during the day and highest during the night. In one instance, gas-to-particle condensation of $(NH_4)_2SO_4$ was observed on all measured particles within a strong SO_2 plume arriving at T1 from the northwest. Particles with high NH_4Cl mass fractions were identified during early morning periods. A limited number of particles (~5% of the total number) with mass spectral features characteristic of biomass burning were also identified.

1 Introduction

To accurately model the radiative forcing of aerosol particles, one must measure in real-time the size, shape, density, chemical composition, and mixing state of ambient particles. This is a formidable challenge because the chemical and physical properties of the aerosol particles are highly complex, dependent on the emission sources, the geography and meteorology of the surroundings, and the gas phase composition of the regional atmosphere. As a result, aerosol particles continually change as they are transported through the atmosphere. Without a detailed understanding of the sources and atmospheric processes that control the chemical and physical transformations of the particles, the influence of aerosol particles on climate remains highly uncertain. Currently, uncertainties in the evaluation of aerosol direct and indirect radiative effects are the source of the largest uncertainty in estimating the overall radiative forcing of the climate (IPCC, 2007).

Urban areas produce large quantities of aerosol particles together with gas phase precursors that influence secondary aerosol formation. Emissions from the numerous sources within an urban environment cause adverse health effects, reduction in visibility, deposition of chemicals to the ecosystem, and direct and indirect ra-

ACPD
8, 21313–21381, 2008

diative forcing that are evident on local, regional, and global scales (Molina et al., 2007). The MILAGRO (Megacity Initiative: Local and Global Research Observations) field study was conducted in and around Mexico City during March of 2006 (http://www.eol.ucar.edu/projects/milagro/). The aim of the study was to obtain a more complete understanding of the atmospheric transformations that occur within the urban plume as it is transported away from the city. The part of the MILAGRO study described in this manuscript focused on the chemical transformations and source apportionment of the aerosol particles.

Until recently, available real-time quantitative instrumentation could provide only an average chemical composition for the ambient aerosol particle ensemble. To evaluate the radiative effects of the aerosol particles and to begin to identify their sources, average data are not necessarily adequate. Consider for example two aerosol particles, one composed of purely carbonaceous material (organic carbon and elemental carbon or soot), and the other composed of purely inorganic material. The hygroscopity, cloud condensation nuclei (CCN) activity, and optical properties of these two (externally mixed) aerosol particles may be significantly different than the hygroscopic, CCN and optical properties of two similar size aerosol particles that are internally mixed (i.e. each particle composed of 50% carbonaceous and 50% inorganic material). Measuring the single particle chemical composition provides the information necessary to determine the ensemble mixing state and analyze the chemical transformations taking place as the particles undergo atmospheric processing. Some of the complexities of particle CCN properties due to coating and mixing are discussed in Sun and Ariya (2006), Petters et al. (2006), and Shilling et al. (2007). The effects on optical properties of particles due to coating, mixing, and aging processes are discussed in Chylek et al. (1995), Fuller et al. (1999), Lesins et al. (2002), Quinn et al. (2005), Baynard et al. (2006), Barnard et al. (2007) and Bond et al. (2006).

A key advance in atmospheric science has been the development of aerosol mass spectrometers that, with on-going improvements and design modifications, can now measure size and chemical composition for individual particles within the ambient en-

semble. (For recent reviews see McMurry et al., 2002; Sullivan and Prather, 2005; Murphy, 2007a; Nash et al., 2006; Canagaratna et al., 2007.) we do not use double parenthesis. One example of such an instrument, featured in this manuscript, is the aerosol mass spectrometer (AMS) developed by Aerodyne Research Inc. (Jayne et al., 2000).

The AMS instrument measures ensemble average chemical composition and size of submicron particles. Recently, the AMS has been redesigned to incorporate two new features that significantly expand the capability of the instrument to provide single particle information. First, the quadrupole mass spectrometer was replaced by a time-of-flight mass spectrometer (TOFMS) (Drewnick et al., 2005; DeCarlo et al., 2006). With the TOFMS coupled to the AMS, single particle mass spectra can be obtained. (This combined instrument is known as a ToF-AMS.) The ToF-AMS can quantitatively measure particle-by-particle, non-refractory aerosol composition as a function of particle aerodynamic diameter. Drewnick et al. (2005) demonstrated the ability of the ToF-AMS to measure single particle mass spectra.

In the second modification, a light scattering module was integrated into the AMS instrument. This version of the instrument is referred to as the LS-AMS (Cross et al., 2007). The light scattering module provides a single particle measurement of scattered light intensity (R_{LS}) for all particles above d_p~250 nm that enter the AMS and impact on the heated vaporizer. A single calibration curve converts R_{LS} to an optical diameter (d_o). Using the relationship between d_o and the simultaneously measured vacuum aerodynamic diameter (d_{va}), the LS-AMS provides a real-time, per particle measurement of the density of the sampled aerosol particles. Further, the LS-AMS provides a quantitative measure of the internal collection efficiency of the AMS by comparing the number of chemically detected particles to the total number of optically detected particles.

The light scattering module has now been added to the ToF-AMS. In this new instrument combination, the acquisition of mass spectra for each particle is triggered by a light pulse scattered by the particle. This instrument is designated as the LS-

ACPD
8, 21313–21381, 2008

ToF-AMS. The LS-ToF-AMS uses thermal desorption and continuous electron impact ionization of single particles, enabling the detection, quantification, and classification of non-refractory, especially organic, fractions of ambient particles. This new approach is unique among current field deployable single particle mass spectrometers, which typically consist of laser-based desorption/ionization instruments that detect refractory material best (e.g. sodium chloride, soot, and dust) (Murphy, 2007a; Nash et al., 2006).

The optical triggering improves the effectiveness and efficiency of the AMS as a single particle mass spectrometer by minimizing the number of data files saved and post-processing steps required to identify individual particles. The presence of the light scattering module does not influence the instrument's ability to measure the ensemble average chemical composition and size distribution. Therefore, the LS-ToF-AMS can measure both ensemble average and single particle properties (e.g. mixing state) of the ambient aerosol by alternating data acquisition modes.

In this article, we present results obtained with the LS-ToF-AMS during the MILAGRO field study in Mexico City in March 2006. The LS-TOF-AMS was located at the T1 sampling site ~40 km NE of the city center. (See the MILAGRO/INTEX-B 2006 special issue of Atmospheric Chemistry and Physics for other results from the MILAGRO field experiment). Typical AMS measurements of submicron, non-refractory aerosol chemistry and chemically-speciated size distributions were obtained from 12–30 March 2006 with several interruptions due to power failures and instrument calibrations. The LS-ToF-AMS successfully characterized the size, chemical composition, and mixing state of individual particles over a 75-h period from 04:27 LT on 27 March to 07:24 LT on 30 March 2006. The ensemble average size and chemical composition were also obtained for this period using the same AMS instrument. This manuscript highlights the results of the single particle measurements made with the new LS-ToF-AMS instrument combination.

1.1 Brief survey of single particle mass spectrometry

Most current, successful single particle mass spectrometers use lasers for particle vaporization and ionization. Among these instruments are the Aerosol Time-of-Flight Mass Spectrometer or ATOFMS (Gard et al., 1997; Su et al., 2004), the Particle Analysis by Laser Mass Spectrometry or PALMS instrument (Murphy and Thomson, 1995; Thomson et al., 2000), the Single Particle Laser Ablation Time-of-flight Mass Spectrometer or SPLAT-MS (Zelenyuk and Imre, 2005) and the Rapid Single Particle Mass Spectrometer or RSMS-II (Phares et al., 2002). While several instruments employ techniques to separate the vaporization and ionization of single particles (e.g. infrared laser pulse for particle desorption prior to ionizing laser pulse for gas phase ionization), most field deployed single particle instruments use either a single excimer or Nd-YAG laser pulse to both vaporize and ionize single particles. This study represents a new approach to single particle mass spectrometery using the AMS thermal vaporization and electron impact ionization techniques.

Single particle mass spectrometers using laser desorption/ionization methods are difficult to quantitatively calibrate (Murphy et al., 2007a, b). Because the high powered laser has to be tightly focused, the detection and ionization efficiency is highly dependent on the shape and size of the particle. Particles with aspherical shapes tend to generate broad particle beams when sampled into vacuum, even with current aerodynamic lensing technology, and thus laser spot size and distance from inlet can control detection efficiency (Huffman et al., 2005). Further, the wavelength and power of the laser used to vaporize and ionize the particles can bias chemical detection (Nash et al., 2006; Murphy, 2007a). For example, species with relatively low ionization potentials (such as potassium) are preferentially ionized and detected. Difficult to ionize species (such as sulfuric or nitric acid) often evade detection. Perhaps even more importantly, the organic ions generated from most laser-based aerosol mass spectrometers are highly fragmented, in many cases to the point of formation of carbon cluster ions. Such fragmentation limits obtainable chemical information (e.g. C:O ratio, organic species

ACPD
8, 21313–21381, 2008

classifications, and elemental carbon versus organic carbon). The measured mass spectrum signal is often non-linear with the mass content of the aerosol particle.

On the other hand, laser ionization single particle mass spectrometers can detect refractory components such as metals, minerals and dust, whereas thermal desorption instruments such as the AMS detect the non-refractory fraction of the sampled particles. Further, some laser-based systems provide high precision vacuum aerodynamic diameter measurements, through the use of two light scattering lasers, and detect significantly smaller particles (>80 nm) by focusing both the light scattering and vaporization/ionization lasers.

The amount of data routinely acquired by any single particle mass spectrometer presents a formidable analytical challenge. For example, Moffet et al. (2008a) acquired 1 million single particle mass spectra over 3.5 weeks of continuous sampling with the laser ablation ATOFMS instrument during the MILAGRO campaign. During the present 75-h study, the LS-TOFAMS sampled ~13 000 single particles and collected 46 GB of single particle data, while simultaneously measuring the average size, chemical composition, and mass of the ambient aerosol ensemble.

In experiments using laser ablation mass spectrometers, hierarchical cluster analysis programs are used to interpret the data. Such programs interrogate the chemical composition, and sort the particles into similar and dissimilar clusters with respect to the mass spectral signals (Song et al., 1999; Murphy et al., 2003; Phares et al., 2001). This methodology simplifies the data set so that a small number of measurable parameters, usually the relative intensity of specific ion signals, can characterize a given cluster. For example, Moffet el al. (2008a) characterized the single particle data set obtained with the ATOFMS instrument at the T0 site using the ART-2a clustering algorithm (Song et al., 1999). For this data analysis, a subset of 24 000 sub-micron and 24 000 super-micron particles were analyzed with ART-2a. The resulting clusters were then matched to the rest of the single particle data set (total of 1 million particles). The clustering algorithm generated 60 sub-micron clusters and 200 super-micron clusters that effectively described 88% of the chemically analyzed single particles. Based on

ACPD
8, 21313–21381, 2008

similarities in the major ion peaks for different clusters, Moffet then generated 15 general particle types by hand from the original 260 clusters and characterized the single particles with respect to this smaller list. While clustering techniques have proven useful at identifying trace components that may point to particle sources (e.g. metals), it has yet to be shown that laser-based instruments and their clustering analysis techniques can provide quantitative measurements of the composition and mixing state of ambient submicron aerosol particles, which are composed mainly of non-refractory organic, sulfate, and nitrate species.

This manuscript describes the first field deployment of a new approach – single particle thermal vaporization mass spectrometry – that may provide useful information on particle chemical compositions, mixing states, and source characteristics that currently cannot be obtained through ensemble measurements or laser-based single particle instruments. Further, the combined LS-ToF-AMS instrument provides a practical method for obtaining to simultaneous ensemble and single particle measurements.

In the AMS instrument, particles impact a heated surface (600°C) and the vaporized components are ionized by electron impact (70 eV). The AMS measures ion signals that are proportional to the total non-refractory particulate mass and thus, the measured signals can be quantified and apportioned into chemical species. Because the single particle mass spectra are analogous to AMS ensemble mass spectra, they are amenable to the same mass spectral deconvolution techniques currently in use for standard, ensemble AMS data. In particular, the single particle mass spectra can be readily analyzed using the standard AMS fragmentation patterns allowing for the classification and calculation of single particle organic and inorganic mass fractions (Jimenez et al., 2003; Allan et al., 2004). Further, the organic fractions can potentially be analyzed using more complicated, and rich, mass spectral deconvolution techniques, such as Positve Matrix Factorization (PMF) (Lanz et al., 2007a).

The current challenges and limitations the LS-ToF-AMS, as deployed in this initial study, are (1) low duty cycle for single particle detection, (2) relatively low signal-to-noise due to high background ion signals in the AMS ionization cage, and (3) the effects

of particle bounce prior to complete vaporization of all non-refractory components. Despite these challenges, meaningful single particle chemical and size information was obtained. The results are presented in the context of the contemporary ensemble measurements using standard AMS operational modes. Specifically, information is presented about source characterization, ensemble mixing state and atmospheric processing.

2 Experimental methods

2.1 Instrumentation

2.1.1 LS-ToF-AMS

A schematic of the ToF-AMS equipped with the light scattering module is shown in Fig. 1. Individual components of the instrument have been described in other publications (Cross et al., 2007; Jayne et al., 2000; Jiménez et al., 2003; DeCarlo et al., 2006; Drewnick et al., 2005). Here we provide a brief overview of the instrument. The LS-ToF-AMS consists of three main sections: (1) aerodynamic lens, (2) particle time-of-flight region, and (3) particle vaporizer together with the TOFMS. As shown in Fig. 1, the light scattering module is located in the particle time-of-flight region between the aerodynamic lens and the vaporizer surface.

In the AMS, particles are sampled from ambient pressure (590 torr at T1 in Mexico City) into an aerodynamic lens through a 130 μm orifice. In their passage through the lens, particles are accelerated by the pressure drop, ~2 torr inside the lens and $<10^{-4}$ torr in the time-of-flight region. The aerodynamic lens focuses particles towards a rotating mechanical chopper, which modulates the particle beam. The chopper is mounted at the front of the particle time-of-flight chamber. The alignment of the 1% chopper slit opening with the particle beam defines t_0 for the particle time-of-flight. At the end of the time-of-flight region, particles impact a heated surface (~600°C) and the

non-refractory species are flash vaporized. The resulting plume of vapor is ionized by electron impact (70 eV) and the ions are transferred to the TOFMS. Mass spectra are acquired and stored in a manner that depends on the mode of operation of the AMS as discussed in Sect. 2.2.

The light scattering module consists of a diode-pumped 405 nm continuous wave 50 mW laser (CrystaLaser, LC BCL-050-405), external mirrors for alignment of the light beam, an ellipsoidal mirror for scattered light collection (Opti-Forms E103-2-01), a razor blade beam stop for quenching the throughput laser light, and a photomultiplier tube (PMT) for scattered light detection (Hamamatsu H6779-00). An optical scattering signal (R_{LS}) is obtained for nearly every particle that impacts the surface of the vaporizer (3.8 mm in diameter) if the particle is larger than the optical size detection limit, in this case d_p~250 nm. As detailed in Cross et al. (2007), this purposeful defocusing of the light scattering laser beam allows for the near complete optical detection of spherical and aspherical particles that impact the vaporizer.

2.2 Data acquisition

Without the light scattering unit, the C-ToF-AMS can operate in three data acquisition modes: Mass Spectrum (MS) mode, Particle Time-of-Flight (PToF) mode, and "Brute Force" Single Particle (BFSP) mode. These modes of operation are described in detail by Drewnick et al. (2005) and DeCarlo et al. (2006). The addition of the light scattering module provides a fourth mode of operation designated as the Light Scattering-Single Particle mode (LSSP). The first two modes are ensemble aerosol measurements, whereas the latter two are single particle modes of operation. The first three modes of operation will be discussed here briefly, the fourth mode will be discussed in greater detail.

During MILAGRO study, the LS-TOF-AMS instrument was sequentially operated in the three modes; MS, PTOF, and LSSP. The sampling time periods for each mode were set corresponding approximately to their duty cycles. The aerosol mass spectrometer measurements presented in this manuscript were saved in 5 min intervals. At

ACPD
8, 21313–21381, 2008

the conclusion of each saving interval, one PToF file, one MS file, and one LSSP file was saved. During the first 150 s of the saving interval, the instrument was alternated every 10 s between MS and PToF modes. During the second 150 s, the instrument was operated in LSSP mode. During each LSSP saving interval, 15 to 30 single particles were sampled (data transferred and saved) depending on the ambient particle concentration. By comparison, in the PToF mode, chemical signals from ~2000 particles were averaged during each 75 s PToF sampling period and ~50 000 particles were averaged in MS mode.

2.2.1 Mass Spectrum (MS) and Particle Time of Flight (PTOF) Modes

As described previously, the TOFMS in the ToF-AMS instruments is a pulsed, orthogonal extraction time-of-flight mass spectrometer. The pulsers were operated at 56 kHz during the MILAGRO study. Thus, the measure of ion signals (i.e. molecules or mass) is determined as a flux of ions in time, similar to the quadrupole aerosol mass spectrometer, rather than the integral of ions from a single event, such as the ablation and ionization of a single particle in a laser-based aerosol mass spectrometer. In the MS mode, the chopper is alternately closed (blocking the particle beam) and opened (typically on a time scale of a few seconds) and full mass spectra are acquired and averaged for each time period. The difference in the ion signals acquired at each *m/z* in the open and closed periods provides the difference mass spectrum for the particle ensemble.

In the PTOF mode, the chopper wheel rotates at a frequency of 130 Hz. During each chopper cycle (i.e. slit to slit), particles enter the time-of-flight chamber through one of two slits in the chopper wheel. The two slits together comprised 1% of the total chopper area. Thus the sampling duty cycle in the PTOF mode is 10^{-2}. A single PTOF data file consists of 300 mass spectra acquired during the ~6 ms of sampling time during a given chopper cycle (each mass spectrum is acquired in 18 μs). Particle velocity is obtained from the measured time interval between the chopper slit opening (t_0) and chemical ion signal (t_f) provided by the vaporized and ionized particle. The vacuum

aerodynamic diameter is calibrated using techniques described in Jayne et al. (2000). In the PTOF mode, particles impact the vaporizer surface individually; however, signals are averaged over many chopper cycles so that average, size-resolved, chemically-speciated mass distributions are obtained.

2.2.2 Brute Force Single Particle (BFSP) Mode

The BFSP mode of ToF-AMS operation is similar to the PTOF mode, except that instead of averaging mass spectra from multiple chopper cycles, the series of 300 mass spectra for each chopper cycle are saved individually. Because the size of the data files saved during BFSP mode (dependent upon # of chopper cycles saved) are significantly larger than the files saved in MS and PTOF modes, it is important to review the mechanism of filtering and saving particle information during single particle experiments.

Without a light scattering module, single particle data be can saved in one of two ways: 1) mass spectra are saved for all chopper cycles regardless of whether a particle entered the AMS during the chopper period or 2) mass spectra are saved only for single particles producing a pre-set sufficiently high chemical ion signal. The former method requires extensive post-processing of large data sets that are mainly zeros. Because the second method depends on setting a threshold for specific *m/z* signals, chemical detection biases can be introduced if the composition of the particles is unknown.

The BFSP mode has been used for instrument calibrations and other laboratory experiments with well-defined particles such as ammonium nitrate particles. The practical application of the AMS as a true single particle instrument for measuring ambient particles required the development of a LSSP mode.

2.2.3 Light Scattering Single Particle Mode (LSSP)

The LSSP mode offers three distinct advantages over the BFSP mode in measuring the mass spectra of single particles. First, instead of saving mass spectra for every chopper cycle (as in the BFSP mode, option 1), the LSSP mode saves mass spectra

ACPD
8, 21313–21381, 2008

only if a light scattering pulse is observed during that chopper cycle. Second, the optical diameter and the vacuum aerodynamic diameter of each particle are measured and from these two parameters, the effective density and total particle mass can be calculated for each particle, independent of the mass spectrometer measurements. Third, the arrival time of the particle at the vaporizer surface can be calculated from the measured particle time-of-flight between the chopper slit and scattered light pulse. This measurement provides information about the efficiency and time-scale of the vaporization/ionization process for each sampled particle.

The two disadvantages of the early version of the LSSP mode used during MILAGRO were (1) only particles larger then a optical detection limit of d_p~250 nm were detected and (2) the actual duty cycle of the LSSP mode as deployed in Mexico was very low, only about 10^{-4} (see below). The first issue was not significant because the LS-ToF-AMS instrument deployed at T1 in Mexico City had a chamber background that limited single particle chemical detection (for an adequate number of *m/z* signals) to approximately the same d_p~250 nm optical diameter threshold (See Fig. 5 in Sect. 3.2).

The low duty cycle was due to the fact that the light scattering signal was collected in the second 2 GHz DAQ channel to ensure direct correlation with the mass spectral signal for each particle. Thus, a significant fraction of the LSSP mode duty cycle was due to transferring and saving the data. This is evident from the following quantitative considerations. The time required to transfer and save the large amount of data obtained for a single particle in the LSSP mode during MILAGRO was about 800 ms. One chopper cycle was about 7 ms. Therefore, the sampling duty cycle of the PToF mode was reduced by about 10^{-2} yielding a LSSP duty cycle of about 10^{-4}. As a consequence, the LSSP data obtained during the 75 h sampling period contains 10^4 fewer particles than the MS mode data (~3000 particles compared to 3×10^7 particles). The efficiency of the LSSP mode of operation is being improved in the second generation of the LS-ToF-AMS.

The optical detection limit, as deployed in Mexico City, was a single value that was conservatively chosen to ensure that all saved data represented real particles. Each

time the light scattering signal triggered a save, 300 mass spectra and the corresponding light scattering signal were transferred from the DAQ board and saved to the hard drive in binary format. Post-processing algorithms were developed to correlate in time the light scattering pulse and chemical ion pulse and to integrate the total ion signal at each *m/z* for the ions produced by the vaporization-ionization of each single particle. Each *m/z* signal of each single particle mass spectrum had separate baseline and signal-to-noise levels that required attention; *m/z*-specific thresholds were derived from signal levels prior to the particle's vaporization and ionization event to identify real particle ion signal from background noise levels. To ensure single particle data quality, multiple consistency checks were done as described in Sect. 3.

Although this preliminary deployment of the LS-ToF-AMS was hindered by low duty cycles and thus low number of single particle recorded events, the data obtained is shown to be useful in determining the mixing state, monitoring the chemical transformations due to atmospheric processing and identifying sources of the particulate matter in Mexico City during the 75 h of single particle data collection. Future implementations of the LS-ToF-AMS DAQ hardware and software are planned that will increase the duty cycle of the LSSP mode by about a factor of 10.

3 Single particle analysis

In our current study, about 13 000 single particle mass spectra were recorded and analyzed during the 75-h sampling period. The following information was obtained for the individual particles: vacuum aerodynamic diameter (d_{va}), optical diameter (d_o), and chemical composition. Multiple internal consistency checks were performed on the single particle data to ensure the data acquisition and processing quality. The correlated single particle measurements of d_{va}, d_o and chemical ion signals provided comparison between two independent measures of total particle mass. The chemical compositions of the single particles were analyzed using standard AMS analysis techniques. Knowing the sampling duty cycles for the LSSP and PTOF modes allowed a

ACPD
8, 21313–21381, 2008

direct comparison between the average LSSP and PTOF mass distributions and tested the capability to measure single particle chemical compositions (i.e. mass fractions). In a few cases two particles of distinct composition and size entered the AMS during a single slit opening. The observation of particle coincidence in the system demonstrated the capability and power of the LS-ToF-AMS to determine the mixing state of ambient aerosol.

3.1 Single particle collection and detection

It has been demonstarted that the AMS does not detect all non-refractory particles that impact the vaporizer surface most likely because the particles bounce off the heated surface without vaporizing (Matthew et al., 2008). Laboratory experiments show that the collection efficiency is a function of the particle composition and phase. For example, laboratory-generated particles composed of liquid organics or ammonium nitrate are detected with 100% efficiency. On the other hand, laboratory generated dry ammonium sulfate particles are collected with only ~25% efficiency. The collection efficiency of the AMS in sampling ambient aerosol particles has been reported to be ~0.5 (Alfarra, 2004; Drewnick et al., 2004; Hogrefe et al., 2004; Takegawa et al., 2005; Zhang et al., 2005a). This mass-based collection efficiency was obtained by comparing the non-refractory mass (typically sulfate) measured by the AMS to the mass collected by co-located instruments such as a Particle-into-Liquid-Sampler (PILS). The collection efficiency of the LS-TOF-AMS used during the MILAGRO campaign was also determined to be ~0.5 by comparisons with co-located SMPS-derived mass distributions and black carbon measurements, and with direct comparison with Aerodyne's C-ToF-AMS on the mobile laboratory during a two day T1 visit (Herndon et al., 2008).

The light scattering module counts and optically sizes all particles of diameter greater than d_p~250 nm whether they produce a chemical ion signal or not. By comparing the total number of chemically detected particles to the total number of optically detected particles, a count-based, self-contained collection efficiency for the AMS is obtained.

During the 75-h of single particle sampling, ~49% of all optically detected particles

produced a measurable chemical ion signal while the remaining ~51% did not produce a clearly detectable chemical signal. This count-based collection efficiency is close to the mass-based collection efficiency of ~0.5. However, we note that the count-based and mass-based collection efficiencies do not provide identical mesurements. The optical module detects both refractory and non-refractory particles (d_p>250 nm) while the mass-based measurement detects only the non-refractory material within ambient particles (30–1000 nm d_{va}).

Because the time-of-flight between the chopper opening and the optical scattering signal is measured in the LSSP mode of operation, additional important information about the nature of the particle vaporization-collection process is obtained. Specifically, this measurement allows one to calculate the arrival time of each particle at the vaporizer surface. In this way, the calculated arrival time of the particle at the vaporizer and the observed time of the chemical ion signal can be compared. Based on this comparison, particle vaporization can be separated into three categories: prompt, delayed, and null vaporization events. Prompt particle events are those that produced a chemical ion signal within 200 μs of impacting the vaporizer surface. The 200 μs limit was chosen based on the timing uncertainty due to the chopper slit width (~70 μs) and the possibility that particles may strike the inverted cone shaped vaporizer more than once prior to full vaporization. Delayed particle events produce a chemical ion signal peak >200 μs after the calculated arrival time at the vaporizer. Clearly, these delayed particles do not vaporize upon initial impact with the heater, but most likely bounce and then vaporize upon secondary impacts with hot ionizer cage surfaces. In the null events, particles strike the vaporizer surface but do not produce a clear chemical ion signal. On a particle by particle basis, the chemical ion signals produced by null particle events are nearly indistinguishable from the mass spectrometer noise. However, when averaged, the total ion signal contribution from the null events is a few percent of the total. In the Milagro study the number fractions of the prompt, delayed, and null particle events were 0.23, 0.26, and 0.51, respectively. The prompt particles contained 59% of the total measured single particle mass, whereas the delayed and null particles

ACPD
8, 21313–21381, 2008

contained 38% and 3%, respectively.

The chemical detection collection efficiency results show a slight particle size dependency. Figure 2 shows the number-based collection efficiencies as a function of particle time-of-flight (proportional to d_{va}) for all the particles detected. The fraction of prompt particles detected decreases with increasing particle size (d_{va}), while the fraction of delayed particles increases with increasing particle size. These inversely related results appear to indicate that larger particles are more prone to bounce prior to full vaporization, likely due to greater momentum of the larger particles. The null particles constituted the largest fraction of the total particles detected and also exhibited a size-dependency similar to the delayed fraction, with greater number of null particle events for larger particles.

The percentage of the total particle mass (from chemical ion signals) detected from the prompt particle events was, on average, higher than that from particles with delayed vaporization. This is illustrated in Fig. 3a and 3b that show the measured single particle mass obtained via calibration from the sum of all ion signals measured with the mass spectrometer for prompt and delayed particles, respectively. In each plot, the mass obtained from the chemical measurement is plotted against the single particle mass (m_p) derived from the measured d_{va} and d_o: $m_p = \pi/6 \times d_o^2 \times d_{va}$. The HOA mass fraction of each particle is shown by the color of the data points in each figure.

The data displayed in Fig. 3a and 3b show considerable scatter due to measurement uncertainties discussed below in Sect. 3.1.1. Still, certain features are clearly evident. As is shown in Fig. 3a for the prompt vaporization events, the two independent measures of single particle mass are clustered near the 1:1 line. A linear fit of the data yields slope of 0.81 (intercept <2 femtograms; R^2=0.5). The data in Fig. 3a exhibit a significant scatter that is correlated with the HOA mass fraction in the particle. The ensemble HOA mass fraction (discussed further in Sect. 4.2) is correlated in time with particulate elemental carbon and gas phase CO measurements. These correlations, together with other published observations (Canagaratna et al., 2004; Zhang et al., 2005b, 2005c), indicate that HOA containing particles typically contain fractal-

ACPD
8, 21313–21381, 2008

like elemental carbon cores. This nonspherical, refractory material does not produce a chemical ion signal in the AMS and reduces the reliability of the d_o measurement due to shape and light absorption. Removing the particles with HOA content (>10%), increases the slope (0.88) and R^2 (0.57) of the linear fit.

The data obtained from the delayed vaporization events are shown in Fig. 3b. This set of data exhibits significantly larger scatter and lower overall chemical ion signals than obtained from the prompt vaporization events. A linear fit to the data in Fig. 3b has a slope of 0.41 (R^2=0.12), suggesting that the measured chemical ion signals represent only about ~40% of the total particle mass. It is likely that particles with delayed vaporization have struck at least two heated surfaces inside the AMS detection region (the vaporizer being the first) and in most cases were not completely vaporized within the 6 ms particle time-of-flight detection window. Speculations can be put forth why some particles vaporize promptly and fully while others do not. At this point however, the phenomenon remains unexplained. Partial vaporization makes chemical identification of such particles uncertain. Therefore, in Sect. 4 we will focus only on the particles that had prompt vaporization.

3.1.1 Uncertainty in single particle mass measurements

Figure 3a and 3b exhibit significant scatter that is attributed to uncertainty in the measurements of chemical ion signal, d_{va} and d_o. The standard deviations determined from the binned data are approximately 43%. Uncertainty in the chemical ion measurement was determined by analyzing the single particle response of the instrument to known size ammonium nitrate and di-octyl sebacate particles. In laboratory calibration experiments, the variance in single particle ion signal (sum of nitrate ions and organic ions for each particle) for the two different particle types was found to be ±10%. The signal-to-noise from the single particle chemical ion signals made during the MILAGRO study were further limited by rather high chamber background signals during the field deployment (single particle chemical ion signals are difference measurements).

The diameter-derived particle mass is influenced by uncertainties in the d_{va} and

d_o measurements. Uncertainty in the d_{va} is due to the timing uncertainty from the 1% chopper. With a 1% chopper slit and a chopper frequency of 130 Hz, the timing uncertainty is ~70 μs which corresponds to a maximum uncertainty in d_{va} of 13%. Uncertainty in the d_o determination is caused by two factors. First, the spread in the light scattering signals caused by some particles passing through the center and others through the edges of the laser beam (laboratory studies have shown that spherical particles exhibit 11% uncertainty in scattered light signal; nonspherical particles will exhibit a higher uncertainty). Second, the calibration curve used to convert scattered light into an optical diameter is based on NH_4NO_3 particles. For particles with a refractive index that is different from the refractive index of NH_4NO_3, an uncertainty in d_o is introduced. For the range of refractive indices expected in the MCMA (real refractive indices of 1.4–1.6, Seinfeld and Pandis, 2006), the uncertainty in d_o is ~10% (Cross et al., 2007). The uncertainties in d_o due to refractive index and particle position in the laser each get doubled in the conversion to particle mass, causing the overall uncertainty in optical diameter derived mass to be ~40%. This uncertainty is an underestimate due to the known presence of black carbon particles, which absorb light at λ=405 nm (the λ of the detection laser in the LS-ToF-AMS). The uncertainty in the diameter-derived mass likely accounts for much of the variance in Fig. 3a and 3b. Variations in the diameter-derived single particle mass will not affect the measurement of single particle chemical composition.

3.2 Single particle chemical composition

Single particle mass spectra were analyzed using the standard AMS approach based on a priori information of the fragmentation patterns of inorganic and organic species (Allan et al., 2003). This technique identifies inorganic species (ammonium, nitrate, sulfate, and chlorides) and separates their mass spectral signals from particulate organic signals.

The mass spectra of the organic fraction are more complex and require more rigorous deconvolution techniques. Because the single particle mass spectra are analo-

gous to AMS ensemble mass spectra, they are in principle amenable to more complicated mass spectral deconvolution techniques currently being developed and applied to standard AMS mass spectra. These techniques include principle component analysis (PCA) (Zhang et al., 2005b) and positive matrix factorization (PMF) (Lanz et al., 2007a, 2007b; Ulbrich et al., 2008). Two of the major types of organic species identified through the use of these multivariate analysis techniques are oxygenated organic aerosol (OOA) and hydrocarbon-like organic aerosol (HOA). HOA particles are strongly correlated with primary aerosol originating from fossil fuel combustion sources. The OOA particles are most likely secondary organic aerosol (SOA) formed in the atmosphere through the condensation of oxidized low vapor pressure organic gases. These techniques are currently being extended to refine and identify other important mass spectral markers for organic species; for example, biomass burning spectral markers.

The first AMS measurements that separated OOA and HOA were preformed by Zhang et al. (2005b) in the Pittsburgh, PA field study. In those experiments, Zhang and co-workers found a simplified two-component analysis wherein the total mass concentration of organics could be reproduced by a linear combination of mass signals at mass-to-charge ratios *m/z*= 44 (mostly CO_2^+) and *m/z*= 57 (mostly $C_3H_9^+$). The *m/z* 44 signal is associated with OOA compounds and the *m/z* 57 is associated with HOA compounds. An expanded multi-component version of this technique has been applied to more than 30 AMS data sets obtained throughout the Northern Hemisphere midlatitudes (Zhang et al., 2007). More recently, using Positive Matrix Factorization (PMF), Lanz et al. (2007b) and Ulbrich et al. (2008) extended the 2-factorial approach to apportion ambient organic aerosol matter into two classes of oxygenated organics.

Our initial chemical analysis approach was to conduct PMF analysis on the ensemble aerosol mass spectra (MS Mode), ensemble PTOF distribution mass spectra, and single particle mass spectra. However, due to low S/N for signal at each *m/z* and low single particle counting statistics for the single particle data and PTOF size distribution data we have settled on the simple and published method for apportioning the organic fractions into two dominant components using the high S/N *m/z*'s 44 and 57

ACPD
8, 21313–21381, 2008

which have been shown to be the predominant signatures of distinct types of organics, labeled OOA and HOA, respectively (Zhang et al., 2005b). For the ensemble average mass spectra obtained in MS Mode, PMF analysis is used to identify the different organic components.

Comparisons between the 2-factor PMF and 2-component PCA results indicate the both of these methods derive very similar HOA and OOA factors from the ensemble organic aerosol mass spectra, which account for >90% of the variance in the data. Thus, comparisons between the PCA and PMF derived HOA and OOA factors in aerosol loading, size distribution, and single particle measurements are meaningful. Comparisons between two and three factor results for PMF analysis of the ensemble aerosol mass spectra show that a third identified PMF factor is essentially split from the existing HOA component. This third identifiable factor is distinct from the HOA and OOA mass spectra in that it contains significant signal at *m/z*'s 60 and 73. As described in DeCarlo et al. (2008), *m/z* 60 and 73 are good markers for biomass burning aerosol in Mexico City. Thus, for the purpose of this paper, this third factor will be labeled BBOA (biomass burning organic aerosol). The filter used to identify BBOA single particles is described in Sect. 4.3.1.

Figure 4 shows the average single particle mass spectra for the HOA and OOA components (top panels; 4a and b, respectively) and the corresponding PMF factors for HOA and OOA (bottom panels; 4c and d, respectively) from the ensemble analysis. Visual comparison shows a good correlation between the average HOA and OOA mass spectra obtained with the two different deconvolution methods.

A comparison of three OOA and three HOA single particle mass spectra is shown in Fig. 5. The particles were randomly chosen from the sampled particles with the criterion that the particle contains a high organic mass fraction consisting of either OOA or HOA. This figure demonstrates the following features: a). Single particles with d_o~350 nm (300<d_{va}<700 nm; note, d_{va} is a function of particle density) exhibit relatively high S/N for all *m/z* signals <100 amu. b). HOA and OOA particles are readily distinguishable and exhibit characteristic peaks for HOA (*m/z* 57) and OOA

ACPD
8, 21313–21381, 2008

(*m/z* 44 and 18). c) Single particles with d_o~200 nm (or smaller) (250<d_{va}<350 nm) have low S/N at most *m/z*'s and the single particle mass spectra exhibit only a few characteristic *m/z* ion signals. Thus, the size detection limit for single particle chemical ion and optical measurements was approximately the same for the instrument in the present MILAGRO study.

3.3 Comparison of single particle and ensemble measurements

In Fig. 6a we show mass spectrometer ion signals (Hz) as a function of particle time of flight. The ensemble averaged signal (PTOF mode) is shown as a dashed line and the averaged single particle signal (LSSP mode) is shown in red. The size detection limits are evident in Fig. 6a. In the MILAGRO study the LSSP mode detected particles with diameters larger than d_p~250 nm (d_{va}~350 nm or ~3.1×10^{-3} s), whereas the ensemble averaged PTOF signal measured particles down to d_{va}~30 nm (with arrival times at the vaporizer ~1.5×10^{-3} s or greater). This lower size limit is determined by the transmission cut-off for the aerodynamic lens inlet. The single particle signal is subdivided into ions counts obtained from prompt (blue), delayed (green), and null (black) particles. For particles larger than ~d_{va}=350 nm (3.1 ms time-of-flight) the signal measured in the PToF mode is in good agreement with the total signal measured in the LSSP mode. This agreement is shown quantitatively in Fig. 6b which displays the correlation between the LSSP and PTOF signals for arrival times between 3.1–5.5 ms (data between arrows in Fig. 6a). The correlation is linear with a slope of 0.85, indicating that the LSSP mode collected 85% of the PTOF signal.

We note from Fig. 6a and 6b that the LSSP signal is about 15% smaller than the than the signal obtained in the PTOF mode. The missing 15% is likely due to delayed vaporization of particles smaller than the optical size detection limit and therefore are not detected in the LSSP mode. This interpretation is further supported by the fact that at longer times-of-flight (>4.8 ms in Fig. 6a), the average LSSP and PTOF modes agree fully.

The results in Fig. 6a suggest that the PTOF mode provides an accurate measure

of the rising edge of ambient particle mass distributions (i.e. at small particle sizes); however, the PTOF mode broadens ambient mass distributions to larger particle sizes due to delayed particle vaporization events.

A consistency check on the measured single particle chemical compositions was done by comparing the averaged single particle chemical compositions with the chemical compositions measured in PTOF mode (for signal with d_{va}>300 nm). The comparison was performed for organic, nitrate, sulfate, and chloride mass fractions. In all cases, the average chemical composition of the single particle and ensemble PTOF data were the same within experimental uncertainty (±10%).

3.4 Mixing state determination

To illustrate the physical and chemical information obtained with the LS-ToF-AMS, we examine a case when two particles entered the AMS during one chopper opening, recorded at 05:35 LT on 27th March – during the morning rush hour. (Under the ambient particle concentrations observed during the experiment, we expect such a two-particle coincidence to occur ~1% of the time). The top panel of Fig. 7 shows the scattered light pulses from the two particles as a function of time-of-flight, with t_0 defined by the opening of the chopper slit. The middle panel shows the corresponding chemical ion signals. The lower panel displays the mass spectrum for each of the sampled particles

The single particle mass spectra in bottom of Fig. 7 clearly show that the chemical compositions of the two sampled particles are distinct. Particle 1 is composed of 100% organic material. The largest mass spectrum component is at m/z=57 characteristic of an HOA particle. Particle 2 is a mixture of oxygenated organics, ammonium nitrate, and ammonium sulfate approximately in equal amounts. The observation of two distinct particle types within the same chopper cycle indicates that the ambient ensemble was externally mixed during this sampling period. Table 1 summarizes the measured chemical and physical properties for these two particles.

The chemical ion pulses in the middle panel of Fig. 7 are separated in time because

ACPD
8, 21313–21381, 2008

the particle exit velocities out of the aerodynamic lens are substantially different due to the difference in effective densities of the two particles. Particle 1 exits the lens with a velocity of 106 m/s and particle 2 with a velocity of 94 m/s. The time separation between the chemical pulses is greater than the time separation between the optical pulses (324 μs versus 198 μs). This difference is due to the additional distance between the laser and vaporizer surface traveled by the two particles. Differences in the vaporization times of the two particles may also influence this time separation (Cross et al., 2007). The ion extraction time is negligible.

The single particle data also provide information about the mass and density of each particle. The mass of particles 1 and 2, as measured by the calibrated mass spectrometer, is 18.2 fg, and 13.0 fg, respectively. The mass composition of particles 1 and 2 (using average densities for the components) yields densities of 0.9 g/cm^3 and 1.5 g/cm^3, respectively. Assuming that the particles are spherical and that all the material in the particles is detected by the mass spectrometer, we calculate the physical diameter of the particle 1 and 2 to be 326 nm and 211 nm, respectively.

The amplitudes of the optical scattering pulses shown in the top panel of Fig. 7 can be used as an independent measure of the particle diameter (denoted as optical diameter d_o). Using the calibration procedure described in Cross et al. (2007) the optical diameters for particle 1 and 2 are 301 nm and 263 nm, respectively. This is within 8% and 20% of the diameters obtained via the mass-density calculations.

An independent calculation of the particle density is obtained from the ratio of the vacuum aerodynamic diameter (d_{va}) and the optical diameter (d_o). That is, $\rho_{\text{eff}}=d_{va}/d_o$. The d_{va} is a function of the physical diameter, the material density, and the shape of the particle. The d_{va} values for particles 1 and 2 are 287 nm and 446 nm, respectively, obtained from the measured particle velocity via a four parameter empirical fit function as described in Bahreini et al. (2003). The densities derived for particles 1 and 2 using the relationship $\rho_{\text{eff}}=d_{va}/d_o$ are 0.95 g/cm^3 and 1.7 g/cm^3, respectively, in reasonable agreement with the chemically-derived densities.

Combining the chemical and physical information collected by the LS-ToF-AMS

from these two particles tells a self-consistent story. Particle 1 was composed of hydrocarbon-like organic matter and exhibited a low effective density. The low effective particle density is consistent with hydrocarbon-like organic (e.g. lubricating oil) densities as well as possibly indicating that Particle 1 was aspherical due to an underlying fractal-like black carbon core. Thus, particle 1 can be identified as a pure HOA particle likely generated from a local combustion source. In contrast, Particle 2 was composed of highly oxidized inorganic and organic matter and exhibited a relatively high effective density consistent with the particle's significant inorganic composition. Particle 2 was an internally mixed accumulation mode particle that likely had undergone significant atmospheric processing prior to detection with the LS-ToF-AMS. The simultaneous observation of these two externally mixed particles illustrates the capabilities of the LS-ToF-AMS technique to provide a measure of the mixing state and atmospheric processing of ambient submicron aerosol particles.

4 Results and discussion

A unique feature of the LS-ToF-AMS is that it provides ensemble as well as single particle measurements. In this section, the composition of the ensemble and single particles measured during the MILAGRO field study are presented and discussed. Information from the two data sets are combined to provide a more complete description of the size, chemical composition, transformations, and mixing state of the ambient aerosol in the Mexico City Metropolitan Area.

4.1 Sampling site and meteorology

The T1 sampling site was located at Tecamac University (19.703 N Latitude and 98.982 W Longitude) at an elevation of 2273 m, ~40 km NE of the Mexico City metropolitan area (MCMA). T0 was the site within city center and T2 was located 35 km N-NE of T1. The location of these three field sites was chosen such that each would

intercept the MCMA plume as it is transported away from the city center to the North (Doran et al., 2008). The area surrounding T1 consists of built up, highly populated residential neighborhoods and less developed regions with open fields. The residential regions are to the south and east of T1. The less developed areas are toward the north and west. A major commuting highway between Mexico City and Pachuca is ~1 km to the east of the site. The LS-ToF-AMS operated in combined single particle and ensemble aerosol modes from 27 to 30 March 2006. The meteorology in the Mexico City basin during these three days was influenced by a "cold-surge" or "Norte" event on 23 March 2006 that brought higher humidities and westerly winds to the Mexico City basin. The mornings at T1 were clear, the afternoons partly cloudy with isolated convection and precipitation events, and the ground level winds favorable for transport from the city center to T1 (Fast et al., 2007 and de Foy et al., 2008).

4.2 Aerosol ensemble properties

The time series of average ensemble mass concentrations separated into organic, nitrate, sulfate, ammonium, and chloride components are plotted in Fig. 8a. As discussed in Sect. 3.2, the measured organic mass was further separated into HOA, OOA, and BBOA components using PMF. The time series for each PMF component is plotted in Fig. 8b. Diurnal plots each species are provided in Fig. 8c and 8d.

The particulate chemical composition and size distribution reflect both the influence of local sources and intense secondary aerosol production. During the day, the ensemble data show three broad features in the organic particulate matter. The first peak occurs during the early morning (04:00–09:00 LT) and is characterized by HOA and BBOA organic compositions. The second peak occurs between 09:00–12:00 LT and consists of a strong particulate nitrate signal combined with HOA, BBOA, and OOA organic contributions. During this time the HOA signal was declining rapidly while the BBOA and OOA signals were increasing. The third broad feature occurs throughout the afternoon and is characterized predominately by OOA organics.

In addition to the ensemble average mass concentrations measured in MS mode, av-

erage size distributions for the major chemical species were obtained while operating the instrument in PTOF mode. The average vacuum aerodynamic diameter size distributions of all the significant non-refractory components are shown in Fig. 9a. These components are: organics, nitrate, sulfate, ammonium, and chloride. The inorganic distributions overlap and appear within the accumulation mode size range, centered at d_{va}~350 nm. The organic size distribution is broader than the inorganic distributions. This difference is attributed to the multiple components of the organic mass. To show this more clearly, in Fig. 9b we plot the HOA and OOA organic components separately (see Sect. 3.2). The HOA distribution is shifted toward smaller d_{va} values compared to the distributions of all other components. This is likely due to the low material density (~0.9 g/cm^3) and potentially non-spherical shape of HOA particles. (Recall d_{va} is proportional to particle density.) By contrast, the density of OOA particles is typically higher (1.3–1.5 g/cm^3) and these particles tend to be more spherical resulting in larger d_{va} values. These two size modes have been classified previously as the "traffic" and "accumulation" modes, respectively (Canagaratna et al., 2007). Because of the overlap between their respective size distributions, it is often assumed that the OOA particles are internally mixed with the inorganic species. On the other hand, based on the difference in their size distribution, the HOA particles are usually assumed to be externally mixed with respect to the inorganic and OOA species.

It is important to note that with only ensemble average size distributions available, the mixing state of the ambient ensemble is assumed, not directly measured. For the particle size-range detected in the LSSP mode (particles with d_p>250 nm) the single particle data unambiguously show whether the ambient ensemble is externally or internally mixed. Section 4.4 describes the mixing state of the ensemble based on the measurements of single particle compositions.

4.3 Single particle chemical compositions

The AMS measures only the non-refractory chemical composition of submicron aerosol particles. In order to limit any potential effects of particle bounce, prior to full vapor-

ization of the non-refractory component of single particles, we have chosen to analyze only the prompt vaporization single particle events (refer to Sect. 3.1). Comparing the single particle mass measured by chemical ion signals with the mass derived from d_{va} and d_o measurements indicates that approximately 88% of the single particle mass is accounted for by the chemical ion signals (Fig. 3a). The remaining ~12% may be due to refractory material (dust, metals, black carbon, etc.) that the AMS does not measure. While inter-particle variations in this analysis are large, the results are consistent with the total PM composition measurements in the MCMA. Salcedo et al. (2006) reported ~20% of the $PM_{2.5}$ measured near the center of Mexico City in 2003 was refractory material (black carbon and soil). Stone et al. (2008) reported that ~25% of the measured $PM_{2.5}$ carbonaceous material at the T1 site was EC during the period of single particle sampling. Stone (2008) also noted that wind-blown dust and soil were present at T1 as potential sources of particles. Typically, dust and soil particles fall into the super-micron size range, which is not detected with the AMS due to transmission efficiency losses for larger particles (Lui et al., 2007).

As was mentioned in Sect. 3.2, several techniques have been developed to obtain the chemical composition of the aerosol particles from their mass spectral measurements. In the current analysis the mass spectra of the non-refractory aerosol composition were initially separated into organic and inorganic species using the method of Allan et al. (2003). The organic fraction was separated into HOA and OOA components using the simple two component PCA algorithm of Zhang et al. (2005b).

In addition to the HOA and OOA anlysis, we explored other single particle filters based on specific *m/z* signals in the mass spectra that identify unique particle types. For example, several organic particles were observed that were dominated by unique organic *m/z* signals at *m/z*=69, 119, and 169. The spectra, not shown, matched previous examples of high temperature lubricating oil (such as Fomblin pump oil), likely from an instrument pump used at the T1 site for sampling purposes. Fifteen Fomblin particles (0.5% of the particles) were identified. These particles were removed from further analysis. An additional single particle filter was used to identify single particles

characteristic of biomass burning organic aerosol (BBOA).

4.3.1 Biomass Burning Organic Aerosol (BBOA) Particles

Specific attention was paid to the identification of biomass burning particles. Several published accounts of strong biomass burning influence in the Mexico City basin during the MILAGRO study suggest that biomass burning is an important source of particles in this region (DeCarlo et al., 2007; Yokleson et al., 2007; Moffet et al., 2008a). To investigate potential signatures of biomass burning in the single particle mass spectra, a single particle filter based on *m/z* marker peaks at 39 (potassium) and 60 and 73 (levoglucosan) was used (DeCarlo et al., 2008; Alfarra et al., 2007; Schneider et al., 2006). Levoglucosan (1,6-anhydro-β-D-glucopyranose), the pyrolysis product of cellulose, is a well-established marker for the combustion of biomass materials (Simoneit, 2002). Once partitioned into the particle phase, levoglucosan does not degrade, making it a useful tracer for long-range transport of biomass burning aerosol (Fraser and Lakshmanan, 2000). In total, 139 single particles were identified as having significant BBOA content (~5% of the particles).

The BBOA factor obtained from the average ensemble measurements shown in Fig. 8 suggests that more than 5% of the nonrefractory aerosol mass could be contributed to biomass burning sources (the BBOA factor has yet to be established as a quantitative measure of biomass burning particulate matter). The number of detected single particles with significant BBOA content may have been suppressed relative to other accumulation mode particles because the markers for biomass burning are (1) potassium ions at *m/z*=39, which are formed via a different ionziation process (i.e. surface ionization) and (2) levoglucosan markers at *m/z*=60 and 73, which exhibited low S/N for smaller particles as discussed in Sect. 3.2. While the absolute magnitude of biomass burning sources may not be adequately represented in the current data set, our single particle measurements indicate that biomass burning was a relatively minor source for particluate matter at T1 during the sampling period under discussion.

The meteorological conditions and co-located measurements of biomass burning

ACPD
8, 21313–21381, 2008

markers at T1 (Stone et al., 2008) are consistent with lower BBOA concentrations during the period of single particle sampling. BBOA particles observed at T1 could have been produced by wildfires and/or urban biomass burning sources. During the period of single particle sampling (27–30 March), the regional meteorology was characterized in the afternoon by increased cloudiness and precipitation over the central plateau (Fast et al., 2007 and de Foy et al., 2008). As a result, the intensity and number of wildfires influencing the area were significantly lower than the previous three weeks (see Fig. 14b, Fast et al., 2007). Stone et al. (2008) measured average levoglucosan concentrations from 18–22 March and 23–30 March at the T1 site. During the earlier time period the levoglucosan concentration was found to be 217 ng/m^3 while in the later time period (coinciding with our single particle sampling) the concentration decreased to 55 ng/m^3.

The 139 single particles with significant BBOA composition were not included in the HOA and OOA analysis. With these particles removed, the reconstructed organic (HOA+OOA) accounted for 93% (R^2=0.84) of the measured single particle organic mass, suggesting that HOA and OOA give a reasonable, but not complete, description of the organics at T1. Since the BBOA SP filter removed organic particles with significant BBOA character, it is possible that some BBOA organic mass remains within the internally mixed single particles detected. This would prevent the HOA and OOA deconvolution technique from describing 100% of the of measured organic mass.

4.3.2 Inorganics

Single particle measurements of ammonium with the AMS were subject to high noise due to interference from background water vapor within the AMS chamber. Despite this challenge, ammonium was measured with reasonable accuracy for single particles with large amounts of ammonium nitrate, sulfate, and/or chloride (~50% by mass). For smaller levels, the NH_4 content of the single particles can be systematically underestimated. As a result, in most cases the uncertainty in NH_4 is the largest source of scatter in the calculation of the single particle mass fractions. Full neutralization of inorganic

species has been previously observed during the dry season in the MCMA (Moya et al., 2003). The ensemble average measurements at T1 indicate that the inorganics present were fully neutralized. Based on this observation and on mass balance, we will assume that the inorganics were in the form of NH_4NO_3, $(NH_4)_2SO_4$, and NH_4Cl. The NH_4 content of each single particle is therefore calculated from the measured single particle mass of nitrate, sulfate, and chloride, unless otherwise stated.

4.4 Mixing state of the ambient aerosol

The fractional compositions of all single particles measured during the 75 h of sampling are plotted in Fig. 10. The data are presented in five panels showing the mass fraction of HOA, OOA, NH_4NO_3, $(NH_4)_2SO_4$, and NH_4Cl for each particle, plotted as a function of the local sampling time. Each panel shows the measured single particle mass fraction of the designated chemical component. That is, every particle is plotted in each panel. The solid black trace plotted in each panel is the 30 min average of the corresponding single particle mass fraction. The vertical black lines denote midnight on each of the sample days.

The majority of the single particles sampled at T1 were internal mixtures of more than one chemical component. This is evident from the lack of substantial numbers of particles in Fig. 10 with mass fractions of any single component equal to 1. This observation is important as it provides insights into the rate of atmospheric processing of particles in the Mexico City basin and has implications for better understanding the ultimate fate and atmospheric effects of primary particles. The single particle data directly confirm assumptions that are typically drawn from ambient, ensemble sampling of size-resolved aerosol chemistry where the average chemical compositions of particles appear to be relatively constant as a function of particle size (Salcedo et al., 2006). This observation also has implications for the classification of single particles by single particle techniques.

For example, Fig. 10 shows that most of the ambient particles measured at T1 contained ammonium nitrate. The range of single particle NH_4NO_3 mass fractions

was ~0.2–0.3 throughout the day and nighttime periods with the exception of higher NH_4NO_3 fractions observed in the late morning. This observation is strongly supported by the single particle mass spectra reported by Moffet et al. (2008a) for ATOFMS results obtained at the T0 site. Nearly all classified single particle types reported exhibit both NO_2 and NO_3 ions (see Fig. 2 in Moffet et al., 2008a). A slightly larger mass fraction range is observed for the OOA and $(NH_4)_2SO_4$ content of the single particles compared to the NH_4NO_3 content. Due to limited signal-to-noise levels in this preliminary version of the LS-ToF-AMS, we will not attempt to interpret whether the observed range in chemical compositions is real or artifact. Instead, we will focus on (1) the atmospheric processes that are apparent from the changing chemical compositions of single particles as a function of time of day and (2) the externally mixed particles that are apparent as their chemical compositions lie outside of this rather narrow range of internally mixed particles.

Figure 10 shows that the chemical compositions (highlighted by the 30 min averages) of ambient particles were dominated by different chemical components throughout the day. During the morning (~1 h after sunrise), the NH_4NO_3 fraction of all single particles rapidly increased, peaking between 10:00–11:00 LT before rapidly declining in the early afternoon; The OOA mass fraction of the single particles increased gradually during the daylight hours, reaching a peak in the middle of the afternoon. The single particle $(NH_4)_2SO_4$ fractions were highest during the evening and overnight and included one instance of a peak in $(NH_4)_2SO_4$ during a strong plume event. In addition to these internally mixed chemical compositional changes, Fig. 10 also shows evidence for externally mixed single particle chloride events occurring between 00:00–10:00 LT each day.

The most obvious exception to the observed internal mixing (in addition to the chloride particles) is the subset of single particles in Fig. 10 with high HOA mass fractions. These particles were observed in highest number concentrations each day during the early morning rush hour with a secondary peak in number concentration apparent during the late evenings. The HOA component measured by the AMS has been shown to

ACPD
8, 21313–21381, 2008

be correlated with primary emissions (Zhang et al., 2005b; Canagaratna et al., 2007). Ensemble HOA data at T1, obtained while operating the instrument in MS-Mode, show that the HOA factor was strongly correlated with measurements of CO and elemental carbon (EC). In agreement with our observations, the results from Moffet et al. (2008a) indicate that the only class of particles observed by the ATOFMS that did not contain nitrate was classified as "EC" particles. The "EC" particles observed at T0 were likely the same type of local, traffic-related combustion-generated particles as the HOA particles described here, as primary traffic-related particles typically contain black carbon and hydrocarbon-like organic matter due to unburned lubricating oil, the major non-refractory component of diesel emissions (Canagaratna et al., 2007; Sakurai et al., 2003). These correlations confirm that the ensemble HOA measurements were associated with primary emissions in Mexico City. In the case of single particles with significant HOA compositions, these particles can be classified as primary emission particles which were likely emitted into the atmosphere as HOA and EC containing particles and subsequently may have undergone atmospheric processing (gas-to-particle condensation or particle coagulation). An important aspect of urban air pollution is the processing and ultimate fate of primary emissions. A specific example is the fate of primary combustion particles that contain black carbon. With increased residence time in the atmosphere, black carbon particles are coated with secondary inorganic and organic condensates that dramatically change the optical, hygroscopic and CCN properties of the original particle (Bond et al., 2006; Ramanathan and Carmichael, 2008). The morphology and relative composition (i.e. black carbon core + unburnt lubricating oil) of combustion particles will depend on the condition of the engine as well as atmospheric variables such as temperature and pressure. Since Mexico City is located at a high altitude, combustion sources will burn more fuel-rich, resulting in elevated contributions from non-refractory chemical components in the emissions from vehicles. Thus, tracking particles with measurable HOA content provides a new method for classifying and characterizing primary, combustion-related particles and their subsequent atmospheric processing.

ACPD
8, 21313–21381, 2008

The color scheme for the points in all panels of Fig. 10 was chosen with this in mind and indicates the HOA content of each particle. Thus, particles colored blue have high-HOA content, particles colored red have low-to-zero-HOA content, and particles colored purple (i.e. red+blue) have intermediate-HOA content with mass fractions. While the total number of measured particles was rather small in the current sample, Fig. 10 explicitly shows that the high-HOA content particles were observed from ~20:00 to 09:00 LT every day. After 09:00 and before ~20:00 LT, the high-HOA particles were not measured, indicating that the "fresh" HOA combustion particles were not observed during day-light hours. This observation is consistent with rapid photochemical activity coating the "fresh" HOA particles during the day with photochemical products (or through particle coagulation). In the following section, we investigate the evolution of these primary particles' number, number fraction, and chemical composition as a function of the time-of-day.

4.4.1 Primary HOA particles and their processing

All of the single particles measured and analyzed were separated into the following categories in accord with the color scheme shown in Fig. 10: (1) High-HOA – considered unprocessed primary particles, (2) Intermediate-HOA – considered processed primary particles, and (3) Low-HOA – considered accumulation particles, not definitively linked to primary (e.g. local combustion) sources. Figure 11 (lower panel) shows the number of single particles as a function of their HOA mass fraction and exhibits a bi-modal distribution with a small mode peaking at HOA mass fraction of ~1.0 and a larger mode centered at HOA mass fraction ~0.05. Single particles with HOA mass fractions equal to zero were not included in the figure or the subsequent analysis under the assumption that they were not primary, traffic-related particles. Figure 11 (upper panel) shows the average mass fractions of NH_4NO_3, $(NH_4)_2SO_4$, NH_4Cl and OOA. The NH_4Cl content remained low, less than 0.10 across the full range of HOA mass fractions reflecting the relatively minor contribution of this compound to the total primary particle chemical composition and mass. On the other hand, the average NH_4NO_3, $(NH_4)_2SO_4$ and

OOA content of the particles increased with decreasing HOA mass fraction implying that these species did influence the primary particle composition.

Combining the information in the top and bottom of Fig. 11 and the uncertainty measurements from Sect. 3.1.1, the "fresh" HOA, combustion-generated particles are defined as particles with mass fractions greater than ~0.90 HOA. The larger mode at low HOA mass fractions represents HOA particles that have undergone significant atmospheric processing (i.e. internally mixed accumulation mode particles). Due to the limited number of total single particles sampled, we have chosen to characterize the processing of "fresh" HOA particles by tracking the number and chemical composition of primary particles with HOA mass fractions between 0.10–0.90. This chosen range may contain particles influenced by more regional (i.e. slower) atmospheric processing, complicating our interpretation of localized processing of primary particles with time frames from minutes to hours.

The diurnal trends of the number of high-HOA, intermediate-HOA and low-HOA particles are displayed in Fig. 12a as a stacked plot. The number of particles in all categories decreased between 11:00–13:00 LT due to dilution caused by the rising boundary layer. The single particle data show that the numbers of high-HOA and intermediate-HOA particles were largest in the early morning (04:30–07:30 LT). The single particle data explicitly show that the number of high-HOA particles decreased to zero during the late morning while the number of intermediate-HOA particles remained relatively constant. As mentioned previously, the high-HOA particles originate from local combustion sources and build up in the atmosphere during the early morning hours. This is consistent with the meteorological conditions: low boundary layer (inhibiting dilution of local emissions) and low photochemical activity (i.e. low production of secondary condensable species). The disappearance of high-HOA particles in the late morning (while the boundary layer was still relatively low, but after the sun had risen) suggests that the high-HOA particles were coated with secondary nitrate. This description of primary particle processing is not possible with ensemble HOA data alone and is consistent with ATOFMS measurements at the T0 site that show sec-

ACPD
8, 21313–21381, 2008

ondary nitrate species on traffic particles between 09:00–15:00 while pure traffic (EC) particles are detected prior to 09:00 (see Fig. 8 in Moffet et al., 2008a). Rapid processing of primary particles in the MCMA has also been reported from single particle microscopy methods (Johnson et al., 2005; Adachi and Buseck, 2008).

To illustrate the connection between primary, HOA single particles and ensemble HOA measurements, we include the diurnal trend for ensemble HOA mass as the dashed grey line in Fig. 12a (μg/m^3 plotted on the right-hand axis). The sum of the high-HOA and intermediate-HOA single particles follows a diurnal trend that is similar to ensemble HOA data. The fact that the HOA factor in the ensemble data has a similar trend and does not go to zero, as does the "fresh" HOA single particles, supports the claim that the primary, HOA single particles and the ensemble HOA factors are related.

To quantify the mixing state of the ambient ensemble, the data in Fig. 12a are replotted in Fig. 12b in terms of the number fraction of each particle type. The data show that during the early morning rush hour ~30–40% of the particles are high-HOA or intermediate-HOA (light and dark blue traces). Prior to sunrise, ~10% of the particles are high-HOA. Once the sun has risen (~09:00 LT), the high-HOA particles disappear while ~20% of the particles remain as intermediate-HOA (coated or processed HOA). During the evening rush hour, a second peak in the fraction of intermediate-HOA particles is observed comprising ~25% of the particles. After the sun has gone down (~20:00), the high-HOA particles reappear making up 5–10% of the particles. The majority (70–80%) of the particles detected are classified as low-to-zero-HOA particles, characteristic of internally mixed (e.g. processed) accumulation mode particles.

Influence of atmospheric processing on particle composition

To track the chemical transformations of the single particles as a function of the time-of-day we show the number fraction of particles containing NH_4NO_3, $(NH_4)_2SO_4$, NH_4Cl, and OOA in Fig. 13a and 13b. Figure 13a displays the diurnal trends for intermediate-HOA particles while Fig. 13b shows the diurnal trends for the low-to-zero-HOA particles. Particles with component mass fractions greater than 0.10 are counted as parti-

ACPD
8, 21313–21381, 2008

cles that contain that chemical component.

The upper panel of Fig. 13a and b is a replot of the data in Fig. 12a. The solid line shows the total number of intermediate-HOA particles (a) or low-to-zero-HOA particles (b). The broken line (same in both Fig. 13a and 13b) is the number of high-HOA particles plotted with respect to the right-hand axis. This plot is presented to remind the reader that the high-HOA particles disappeared in the late morning after ~09:00 LT.

With the onset of photochemical activity (09:00–12:00 LT), the number of intermediate-HOA particles that contain NH_4NO_3 increases from 80% to 100%. Likewise, an increase from 95% to 100% of the low-to-zero-HOA particles that contain NH_4NO_3 is observed between 09:00–12:00 LT. The fact that all single particles measured between 09:00–12:00 LT contained NH_4NO_3 suggests rapid condensation of secondary nitrate onto all pre-exisiting particles. Given the distance of likely high-HOA particle source from T1 (the highway ~1 km away) and the average wind speed and direction, we calculate that the primary HOA particles were coated with NH_4NO_3 in ~15–30 min during this time period. We note that the fraction of intermediate-HOA particles containing NH_4NO_3 decreased back to ~80% after 12:00. The rise and fall in fraction of particles with ntirate was due to the temperature-dependent equilibrium constant in the reaction: $NH_{3(g)}+HNO_{3(g)} \leftrightarrow NH_4NO_{3(s)}$. The MCMA atmosphere contains high concentrations of gas phase NH_3. Nitric acid is formed from reaction of NO_2 and photochemically-produced OH radicals. Therefore, with sufficient sunlight to produce OH radicals, HNO_3 will be form in a single oxidation step. In the early morning at T1, the temperature was low, resulting in conversion of the HNO_3 to NH_4NO_3 which subsequently condensed onto all pre-existing particles. As the temperature increased in the late morning and early afternoon, the dissociation of NH_4NO_3 back to NH_3 and HNO_3 was favored. These results are consistent with the results of Zheng et al. (2008) who monitored the particulate NO_3 and gas phase HNO_3 concentrations at T0.

During the afternoon hours, the number of intermediate-HOA particles infuenced by OOA steadily increases from ~30% (prior to 12:00) to ~55% (12:00–15:00 LT) to ~73% (15:00–18:00 LT). For the low-to-zero-HOA particles, ~90% of the particles contained

ACPD
8, 21313–21381, 2008

OOA in the morning and 100% contained OOA in the afternoon. Rapid formation of secondary organic aerosol in the MCMA region has been previously reported (Volkamer et al., 2006). The single particle data presented here indicate that OOA condenses onto nearly all single particles measured between 15:00–18:00 LT. Unlike the secondary nitrate, secondary organic species typically require multiple oxidation steps prior to forming oxygenated organic aerosol or condensing organic material on pre-existing particles (Kroll and Seinfeld, 2008). During the early morning time period when secondary nitrate formation dominates the single particle composition, the production rate of OOA is slower than in the mid afternoon (Volkamer et al., 2006). The single partice data presented here suggest important temporal differences between secondary inorganic and organic processes that have implications for optical, hygroscopic, and CCN treatments of primary particle processing in urban environments.

Particles that contain $(NH_4)_2SO_4$ were most prevalent during the evening and overnight time periods (18:00–24:00 LT). For the intermediate-HOA particles, ~65% of the particles contained $(NH_4)_2SO_4$ in the late evening and overnight compared to ~36% during the middle of the day. A similar increase was observed for the low-to-zero-HOA particles from ~69% during the middle of the day to ~93% in the evening and overnight. Sulfate has been reported to be a major component of $PM_{2.5}$ in the MCMA (Salcedo et al., 2006; Johnson et al., 2005, 2006; Querol et al., 2008; DeCarlo et al., 2008; Kleinman et al., 2008). The major formation pathway of particulate sulfate is aqueous phase SO_2 oxidation (Salcedo et al., 2006). In the MCMA, SO_2 has significant anthropogenic (the Tula refinery complex and industrial regions concentrated in the northwest) and natural (the active Popocatepetl volcano in the southwest) sources. Given the general lack of spatial variability in sulfate concentrations, sulfate is typically attributed to regional-scale atmospheric processing (Querol et al., 2008; DeCarlo et al., 2008). The single particle observations of a broad range of measured $(NH_4)_2SO_4$ mass fractions and diurnal pattern that peaked in the late evening and overnight are consistent with regional-scale production and accumulation of particulate sulfate. A detailed examination of the single particle $(NH_4)_2SO_4$ content during a SO_2 plume event

at T1 is provided in Sect. 4.4.2.

The fraction of particles containing NH_4Cl was highest for intermediate-HOA and low-to-zero-HOA particles during the early morning hours (00:00–10:00 LT). At this time, ~15–20% of the intermediate-HOA particles and ~30–40% of the low-to-zero-HOA particles contained NH_4Cl. Since the fraction of particles with NH_4Cl was highest during the overnight period it is unlikely that the chloride was formed via photochemical reactions. The lower fraction of particles influenced by chloride suggests that the chloride may have come from a unique source. A detailed discussion of the potential sources of the high chloride containing particles is provided in Sect. 4.4.3.

4.4.2 SO_2 plume event

Returning to Fig. 10 we note that a brief period of high single particle $(NH_4)_2SO_4$ was observed on 28 March at 19:00 LT. Back trajectories for the time period during high single particle $(NH_4)_2SO_4$ indicate that the air was arriving at T1 directly from the northwest. The Tula power plant refinery complex is located ~50 km to the northwest of T1 and has been shown to emit high concentrations of SO_2 into the MCMA region (Johnson et al., 2006; Kleinman et al., 2008; DeCarlo et al., 2008; Fast et al., 2007, Querol et al., 2008). Co-located gas phase measurements at T1 confirmed that the plume measured at this time contained elevated levels of SO_2 (~8 ppb). During the SO_2 plume, 100% of the single particles measured at T1 had $(NH_4)_2SO_4$ mass fractions of 0.60 or greater. The fact that all the particles measured at this time contained elevated levels of $(NH_4)_2SO_4$ suggests that gas phase SO_2 oxidation followed by gas-to-particle condensation or heterogeneous oxidation of SO_2 to SO_4 occurred within the SO_2 plume as it was advected from Tula to the T1 site.

As the conversion from SO_2 to SO_4 is a slow gas phase process (Seinfeld and Pandis, 2006; Stockwell and Calvert, 1983) and its heterogeneous conversion is dependent upon particle chemical compositions, particulate sulfate is often associated with slower, regional-scale atmospheric processing, but this instance of high single particle sulfate was the result of point source emissions rather than regional-scale processing.

Anthropogenic SO_2 emissions, such as the observed Tula plume, have direct effects on the processing or aging of all of the entrained particles and may provide a source for much of the increased sulfate mass fractions during the late evening and overnight time periods.

4.4.3 High chloride content single particles

A second feature in Fig. 10 was the presence of a subset of single particles with high chloride content observed between 00:00–10:00 LT each day. During these times, ~10% of the total single particles sampled had NH_4Cl mass fractions >0.10. The presence of these high chloride particles indicates that these externally mixed particles may have a specific, identifiable source.

During the MILAGRO study, Moffet el al. (2008a, b) used an ATOFMS located at the T0 site to measure the chemical composition of single particles. Results from the ATOFMS show that a large fraction of the total particles sampled between 02:00–05:00 LT each morning were internally mixed Pb-Zn-Cl particles (Moffet et al., 2008b). Given this mixed composition, and the spatial and temporal distribution of PbZnCl particles, Moffet concluded that the early morning chloride particles originated at industrial sites located in the northern region of the city. In addition to industrial sources, potential sources of chloride in the MCMA region include emissions from biomass and trash burning, drinking water, and waste-water treatment facilities (Tanaka et al., 2003).

The single particle measurements made with the LS-ToF-AMS are not chemically sensitive to heavy metal species such as Zn and Pb because the time scale for vaporization of such species is longer than the 6 ms PTOF saving interval. On the other hand, ensemble measurements in MS mode can be examined over longer time scales (minutes) and can help determine if heavy metals are present in the aerosol particles. Close examination of the ensemble data acquired during time periods of high chloride signal indicate that Pb was present in about half of the instances of high particulate chloride. In such cases, the Pb signal was approximately 100 times smaller than the chloride signal. Care must be taken when interpreting AMS measurements of heavy

ACPD
8, 21313–21381, 2008

metals and further characterization of the ionization efficiency of metal species must be done before quantitative information is reported. Nevertheless, on a qualitative basis, these observations suggest that only some of the chloride events at T1 were correlated with Pb, and that when present, lead constituted a relatively minor component of the total particle mass. Lower concentrations of Pb containing particles were also measured at the T1 site relative to the T0 site by Moreno et al. (2008).

Although the single particle detection is not chemically sensitive to metal species, the size information obtained with the LS-ToF-AMS can be used to gain additional insight into the presence of heavy metals in the single particles. The densities of $PbCl_2$ and $ZnCl_2$ are 5.85 g/cm^3 and 2.90 g/cm^3, respectively. If a single particle were predominately composed of these species it would have a significantly higher density than the majority of other submicron ambient aerosol particles (typically ρ=0.9–1.8 g/cm^3). The simultaneous measure of d_{va} and d_o provides a per particle measure of the effective density of all single particles, independent of chemical detection. Examination of all single particles measured during the high chloride particle events show that no particles had effective densities greater than 1.8 g/cm^3. This evidence suggests that if $PbCl_2$ and $ZnCl_2$ were present in the particles, it comprised a relatively minor amount of the total single particle mass. Our results are consistent with the observations of Murphy et al. (2007b) who studied the Pb content of single particles throughout the United States with the PALMS, ATOFMS, and RSMS single particle mass spectrometers. Murphy emphasizes the importance of understanding the chemical detection sensitivity of single particle mass spectrometers. Calibration experiments indicate that the PALMS and ATOFMS instruments are ~12 times more sensitive to metal species than detection of NH_4NO_3 or HNO_3. Therefore, when measuring single particles with any Pb content, it is possible to over-estimate the mass contribution of the metal species to the total particle composition with laser-ablation single particle mass spectrometers.

Our single particle measurements at T1 suggest that the predominant form of chloride in the single particles was ammonium chloride. This is consistent with the meteorological conditions. During the early morning, when the high chloride particles were

ACPD
8, 21313–21381, 2008

observed, the temperature was low and the relative humidity was high, conditions that favor the formation and condensation of more volatile ammonium chloride from reaction of $HCl_{(g)}$ and $NH_{3(g)}$ (San Martini et al., 2006a, b; Salcedo et al., 2006).

Further, a mass balance examination of the NH_4 content of the high chloride particles is consistent with the composition of the particles being NH_4Cl. The identification of the chloride component as NH_4Cl is supported by the data displayed in Fig. 14a. This figure plots the "real" NH_4 mass, measured by the mass spectrometer as a function of the amount of calculated NH_4 required to fully neutralize the per particle inorganic content (i.e. neutralized to $(NH_4)_2SO_4$, NH_4NO_3, and NH_4Cl). The correlation is reasonable (R^2=0.75; slope=0.95). The particles displayed in Fig. 14a have NH_4Cl mass fractions of 0.40 or greater and most were internally mixed with NH_4NO_3. The NH_4NO_3 mass fraction of each particle is indicated by the color of the data points as indicated in the legend. In Fig. 14b we show the mass spectrum for the single particle denoted with an arrow in Fig. 14a. The mass spectrum shows that this particle was predominately NH_4Cl combined with some NH_4NO_3 and very little organic. Based on these observations, we conclude that a significant fraction of the particulate chloride measured with the LS-ToF-AMS at T1 was in the form of NH_4Cl.

5 Summary

We report on the first single particle application of the Aerodyne time-of-flight aerosol mass spectrometer equipped with a light scattering module (LS-ToF-AMS). The LS-ToF-AMS was deployed during the MILAGRO 2006 campaign at the T1 ground site ~40 km northeast of Mexico City. With the LS-ToF-AMS single particle and ensemble average aerosol properties were measured from the same operating platform. While operating in the single particle mode, 12 853 optically-triggered single particle mass spectra were saved and analyzed during 75 h of continuous sampling. Analysis of the mass composition of the single particles allowed the LS-ToF-AMS to provide insights about the mixing state, source contributions and chemical transformations of the ambi-

ACPD
8, 21313–21381, 2008

ent aerosol particles in the MCMA. The following results were obtained in this study:

1. Using the single particle detection capabilities of this instrument, the detection efficiency of the AMS was quantitatively determined.

2. Based on the time required for the particles to be vaporized, ionized and detected, particles were categorized into three types: prompt vaporization, delayed vaporization, and "null" vaporization. Null particles are those detected optically but do not produce a measurable chemical ion signal. Prompt particles made up 23% of the total number and 59% of the total mass. Delayed particles made up 26% of the total number and 38% of the total mass. Null particles made up 51% of the total number and 3% of the total mass. The study shows that the mass content of particles undergoing prompt vaporization is reliably measured. Detailed analysis was preformed for this class of particles.

3. The single particle mass measurement was shown to be in quantitative agreement with average ensemble mass measurements.

4. The single particle mass components were categorized into HOA, OOA, NH_4NO_3, $(NH_4)_2SO_4$, and NH_4Cl fractions and were displayed as a function of sampling time.

5. The measurement of chemical composition allowed the identification of time periods during which the ambient ensemble was externally mixed. In some cases the chemical composition of the particles suggested a likely source.

6. During morning rush hour (04:00–09:00 LT) each day the ambient ensemble was an external mixture of combustion-generated unprocessed HOA particles from local traffic and other particles of mixed composition.

7. From 09:00–12:00 LT all particles within the ambient ensemble, including HOA particles originating from local traffic sources, were coated with NH_4NO_3 due to

ACPD
8, 21313–21381, 2008

photochemical production HNO_3. NH_4NO_3 condensation was more rapid than OOA condensation during the late morning hours.

8. During the afternoon hours (12:00–18:00 LT), OOA condensation occurred, causing an increase in the average single particle OOA mass fraction of the majority of the single particles.

9. During a single time period, gas-to-particle condensation of $(NH_4)_2SO_4$ was observed within a strong $SO_{2(g)}$ plume arriving at T1 from the northwest.

10. Particles with high NH_4Cl mass fractions were identified during early morning periods.

11. Particles with mass spectral features characterized by biomass burning were also identified.

Acknowledgements. The authors gratefully acknowledge A. Laskin and Y. Dessiaterik for use of their SMPS system during instrument calibrations, B. de Foy and J. D. Fast for helpful discussions about the MCMA meteorology, R. C. Cohen for HNO_3 and NO_2 measurements at T1, and G. Huey for SO_2 measurements at T1. This research was supported by the Office of Science (BER), Department of Energy (Atmospheric Science Program) grants No. DE-FG02-05ER63995, DE-FG02-05ER84268, DOE DE-FG02-05ER63982 and the Atmospheric Chemistry Program of the National Science Foundation grant No. ATM-0525355. ESC was funded by the NASA Earth System Science Fellowship program.

References

Adachi, K. and Buseck, P. R.: Internally mixed soot, sulfates, and organic matter in aerosol particles from Mexico City, Atmos. Chem. Phys., 8, 6469–6481, 2008, http://www.atmos-chem-phys.net/8/6469/2008/.

Alfarra, M. R.: Insights into atmospheric organic aerosols using an Aerosol Mass Spectrometer, Ph.D thesis, University of Manchester, Manchester, England, 2004.

Alfarra, M. R., Prevot, A. S. H., Szidat, S., Sandradewi, J., Weimer, S., Lanz, V. A., Schreiber, D., Mohr, M., and Baltensperger, U.: Identification of the mass spectral signature of organic aerosols from wood burning emissions, Environ. Sci. Technol., 41, 5770–5777, doi:10.1021/es062289b, 2007.

Allan, J. D., Jimenez, J. L., Coe, H., Bower, K. N., Williams, P. I., and Worsnop, D. R.: Quantitative sampling using an Aerodyne Aerosol Mass Spectrometer. Part 1: Techniques of data interpretation and error analysis, J. Geophys. Res. Atmos., 108(D3), 4090, doi:10.1029/2002jd002358, 2003.

Bahreini, R., Jimenez, J. L., Wang, J., Flagan, R. C., Seinfeld, J. H., Jayne, J. T., and Worsnop, D. R.: Aircraft-based aerosol size and composition measurements during ACE-Asia using an Aerodyne Aerosol Mass Spectrometer, J. Geophys. Res. Atmos., 108, 8645, doi:10.1029/2002jd003226, 2003.

Barnard, J. C., Kassianov, E. I., Ackerman, T. P., Johnson, K., Zuberi, B., Molina, L. T., and Molina, M. J.: Estimation of a "radiatively correct" black carbon specific absorption during the Mexico City Metropolitan Area (MCMA) 2003 field campaign, Atmos. Chem. Phys., 7, 1645–1655, 2007, http://www.atmos-chem-phys.net/7/1645/2007/.

Baynard, T., Garland, R. M., Ravishankara, A. R., Tolbert, M. A., and Lovejoy, E. R.: Key factors influencing the relative humidity dependence of aerosol light scattering, Geophys. Res. Lett., 33, L06813, doi:10.1029/2005gl024898, 2006.

Bond, T. C. and Bergstrom, R. W.: Light absorption by carbonaceous particles: An investigative review, Aerosol Sci. Technol., 40, 27–67, doi:10.1080/02786820500421521, 2006.

Canagaratna, M. R., Jayne, J. T., Ghertner, D. A., Herndon, S., Shi, Q., Jimenez, J. L., Silva, P. J., Williams, P., Lanni, T., Drewnick, F., Demerjian, K. L., Kolb, C. E., and Worsnop, D. R.: Chase studies of particulate emissions from in-use New York City vehicles, Aerosol Sci. Technol., 38, 555–573, 2004.

Canagaratna, M. R., Jayne, J. T., Jimenez, J. L., Allan, J. D., Alfarra, M. R., Zhang, Q., Onasch, T. B., Drewnick, F., Coe, H., Middlebrook, A., Delia, A., Williams, L. R., Trimborn, A. M., Northway, M. J., Kolb, C. E., Davidovits, P., and Worsnop, D. R.: Chemical and microphysical characterization of ambient aerosols with the Aerodyne Aerosol Mass Spectrometer, Mass Spec. Rev., 26, 185–222, 2007.

Chylek, P., Videen, G., Ngo, D., Pinnick, R. G., and Klett, J. D.: Effect of black carbon on the optical-properties and climate forcing of sulfate aerosols, J. Geophys. Res.-Atmos., 100, 16325–16332, 1995.

Cross, E. S., Slowik, J. G., Davidovits, P., Allan, J. D., Worsnop, D. R., Jayne, J. T., Lewis, D. K., Canagaratna, M., and Onasch, T. B.: Laboratory and ambient particle density determinations using light scattering in conjunction with aerosol mass spectrometry, Aerosol Sci. Technol., 41, 343–359, doi:10.1080/02786820701199736, 2007.

de Foy, B., Fast, J. D., Paech, S. J., Phillips, D., Walters, J. T., Coulter, R. L., Martin, T. J., Pekour, M. S., Shaw, W. J., Kastendeuch, P. P., Marley, N. A., Retama, A., and Molina, L. T.: Basin-scale wind transport during the MILAGRO field campaign and comparison to climatology using cluster analysis, Atmos. Chem. Phys., 8, 1209–1224, 2008, http://www.atmos-chem-phys.net/8/1209/2008/.

DeCarlo, P. F., Kimmel, J., Trimborn, A., Northway, M., Jayne, J. T., Aiken, A., Gonin, M., Fuhrer, K., Horvath, T., Docherty, K., Worsnop, D. R., and Jimenez, J. L.: Field-deployable, high-resolution, time-of-flight Aerosol Mass Spectrometer, Anal. Chem., 78, 8281–8289, 2006.

DeCarlo, P. F., Dunlea, E. J., Kimmel, J. R., Aiken, A. C., Sueper, D., Crounse, J., Wennberg, P. O., Emmons, L., Shinozuka, Y., Clarke, A., Zhou, J., Tomlinson, J., Collins, D. R., Knapp, D., Weinheimer, A. J., Montzka, D. D., Campos, T., and Jimenez, J. L.: Fast airborne aerosol size and chemistry measurements above Mexico City and Central Mexico during the MILAGRO campaign, Atmos. Chem. Phys., 8, 4027–4048, 2008, http://www.atmos-chem-phys.net/8/4027/2008/.

Doran, J. C., Barnard, J. C., Arnott, W. P., Cary, R., Coulter, R., Fast, J. D., Kassianov, E. I., Kleinman, L., Laulainen, N. S., Martin, T., Paredes-Miranda, G., Pekour, M. S., Shaw, W. J., Smith, D. F., Springston, S. R., and Yu, X.-Y.: The T1-T2 study: evolution of aerosol properties downwind of Mexico City, Atmos. Chem. Phys., 7, 1585–1598, 2007, http://www.atmos-chem-phys.net/7/1585/2007/.

Drewnick, F., Hings, S. S., DeCarlo, P., Jayne, J. T., Gonin, M., Fuhrer, K., Weimer, S., Jimenez, J. L., Demerjian, K. L., Borrmann, S., and Worsnop, D. R.: A new time-of-flight Aerosol Mass Spectrometer (ToF-AMS) – instrument description and first field deployment, Aerosol Sci. Technol., 39, 637–658, 2005.

Drewnick, F., Schwab, J. J., Jayne, J. T., Canagaratna, M., Worsnop, D. R., and Demerjian, K. L.: Measurement of ambient aerosol composition during the PMTACS-NY 2001 using an Aerosol Mass Spectrometer. Part I: Mass concentrations, Aerosol Sci. Technol., 38, 92–103, 2004.

Fast, J. D., de Foy, B., Acevedo Rosas, F., Caetano, E., Carmichael, G., Emmons, L., McKenna, D., Mena, M., Skamarock, W., Tie, X., Coulter, R. L., Barnard, J. C., Wiedinmyer, C., and

Madronich, S.: A meteorological overview of the MILAGRO field campaigns, Atmos. Chem. Phys., 7, 2233–2257, 2007, http://www.atmos-chem-phys.net/7/2233/2007/.
Fraser, M. P. and Lakshmanan, K.: Using levoglucosan as a molecular marker for the long-range transport of biomass combustion aerosols, Environ. Sci. Technol., 34, 4560–4564, doi:10.1021/es991229l, 2000.
Fuller, K. A., Malm, W. C., and Kreidenweis, S. M.: Effects of mixing on extinction by Carbonaceous particles, J. Geophys. Res.-Atmos., 104, 15941–15954, 1999.
Gard, E., Mayer, J. E., Morrical, B. D., Dienes, T., Fergenson, D. P., and Prather, K. A.: Real-time analysis of individual atmospheric aerosol particles: Design and performance of a portable ATOFMS, Anal. Chem., 69, 4083–4091, 1997.
Herndon, S. C., Onasch, T. B., Wood, E. C., Kroll, J. H., Canagaratna, M. R., Jayne, J. T., Zavala, M. A., Knighton, W. B., Mazzoleni, C., Dubey, M. K., Ulbrich, I. M., Jimenez, J. L., Seila, R., de Gouw, J. A., de Foy, B., Fast, J., Molina, L. T., Kolb, C. E., and Worsnop, D. R.: The correlation of secondary organic aerosol with odd oxygen in Mexico City, J. Geophys. Res., 15, L15804, doi:10.1029/2008GL034058, 2008.
Hogrefe, O., Schwab, J. J., Drewnick, F., Lala, G. G., Peters, S., Demerjian, K. L., Rhoads, K., Felton, H. D., Rattigan, O. V., Husain, L., and Dutkiewicz, V. A.: Semicontinuous $PM_{2.5}$ sulfate and nitrate measurements at an urban and a rural location in New York: PMTACS-NY summer 2001 and 2002 campaigns, J. Air Waste Manage., 54, 1040–1060, 2004.
Huffman, J.A., Jayne, J. T., Drewnick, F., Aiken, A. C., Onasch, T., Worsnop, D. R., and Jimenez, J. L.: Design, modeling, optimization, and experimental tests of a particle beam width probe for the Aerodyne Aerosol Mass Spectrometer, Aerosol Sci. Technol., 39, 1143–1163, 2005.
Jayne, J. T., Leard, D. C., Zhang, X., Davidovits, P., Smith, K. A., Kolb, C. E., and Worsnop, D. R.: Development of an Aerosol Mass Spectrometer for size and composition analysis of submicron particles, Aerosol Sci. Technol., 33, 49–70, 2000.
Jimenez, J. L., Jayne, J. T., Shi, Q., Kolb, C. E., Worsnop, D. R., Yourshaw, I., Seinfeld, J. H., Flagan, R. C., Zhang, X., Smith, K. A., Morris, J. W., and Davidovits, P.: Ambient aerosol sampling using the Aerodyne Aerosol Mass Spectrometer, J. Geophys. Res., 108, 8425, doi:8410.1029/2001JD001213, 2003.
Johnson, K. S., Zuberi, B., Molina, L. T., Molina, M. J., Iedema, M. J., Cowin, J. P., Gaspar, D. J., Wang, C., and Laskin, A.: Processing of soot in an urban environment: Case study from the Mexico City metropolitan area, Atmos. Chem. Phys., 5, 3033–3043, 2005, http://www.atmos-chem-phys.net/5/3033/2005/.

Johnson, K. S., de Foy, B., Zuberi, B., Molina, L. T., Molina, M. J., Xie, Y., Laskin, A., and Shutthanandan, V.: Aerosol composition and source apportionment in the Mexico City Metropolitan Area with PIXE/PESA/STIM and multivariate analysis, Atmos. Chem. Phys., 6, 4591–4600, 2006, http://www.atmos-chem-phys.net/6/4591/2006/.

Kroll, J. H., and Seinfeld, J. H.: Chemistry of secondary organic aerosol: Formation and evolution of low-volatility organics in the atmosphere, Atmos. Environ., 42, 3593–3624, doi:10.1016/j.atmosenv.2008.01.003, 2008.

Lanz, V. A., Alfarra, M. R., Baltensperger, U., Buchmann, B., Hueglin, C., and Prevot, A. S. H.: Source apportionment of submicron organic aerosols at an urban site by factor analytical modelling of aerosol mass spectra, Atmos. Chem. Phys., 7, 1503–1522, 2007a, http://www.atmos-chem-phys.net/7/1503/2007/.

Lanz, V. A., Alfarra, M. R., Baltensperger, U., Buchmann, B., Hueglin, C., Szidat, S., Wehrli, M. N., Wacker, L., Weimer, S., Caseiro, A., Puxbaum, H., and Prevot, A. S. H.: Source attribution of submicron organic aerosols during wintertime inversions by advanced factor analysis of aerosol mass spectra, Environ. Sci. Technol., 42, 214–220, 2007b.

Lesins, G., Chylek, P., and Lohmann, U.: A study of internal and external mixing scenarios and is effect on aerosol optical properties and direct radiative forcing, J. Geophys. Res., 110, D07S09, 107(D10), 4094, 2002.

Liu, P. S. K., Deng, R., Smith, K. A., Williams, L. R., Jayne, J. T., Canagaratna, M. R., Moore, K., Onasch, T. B., Worsnop, D. R., and Deshler, T.: Transmission efficiency of an aerodynamic focusing lens system: Comparison of model calculations and laboratory measurements for the Aerodyne Aerosol Mass Spectrometer, Aerosol Sci. Technol., 41, 721–733, 2007.

Matthew, B. M., Onasch, T. B., and Middlebrook, A. M.: Collection efficiencies in an Aerodyne Aerosol Mass Spectrometer as a function of particle phase for laboratory generated aerosols, Aerosol Sci. Technol., 42, 11, 884–898, doi:10.1080/02786820802356797, 2008.

McMurry, P. H.: A review of atmospheric aerosol measurements, Atmos. Environ., 34, 1959–1999, 2000.

Moffet, R. C., de Foy, B., Molina, L. T., Molina, M. J., and Prather, K. A.: Measurement of ambient aerosols in northern Mexico City by single particle mass spectrometry, Atmos. Chem. Phys., 8, 4499–4516, 2008a, http://www.atmos-chem-phys.net/8/4499/2008/.

Moffet, R. C., Desyaterik, Y., Hopkins, R. J., Tivanski, A. V., Gilles, M. K., Wang, Y., Shutthanandan, V., Molina, L. T., Abraham, R. G., Johnson, K. S., Mugica, V., Molina, M. J., Laskin, A., and Prather, K. A.: Characterization of aerosols containing Zn, Pb, and Cl from an industrial

region of Mexico City, Environ. Sci. Technol., 42, 7091–7097, 2008b.
Molina, L. T., Kolb, C. E., de Foy, B., Lamb, B. K., Brune, W. H., Jimenez, J. L., Ramos-Villegas, R., Sarmiento, J., Paramo-Figueroa, V. H., Cardenas, B., Gutierrez-Avedoy, V., and Molina, M. J.: Air quality in North America's most populous city – overview of the MCMA-2003 campaign, Atmos. Chem. Phys., 7, 2447–2473, 2007, http://www.atmos-chem-phys.net/7/2447/2007/.
Molina, L. T., Madronich, S., Gaffney J., et al.: An overview of the MILAGRO 2006 Campaign: Mexico City emissions and its transport and transformation, Atmos. Chem. Phys. Discuss., in preparation, 2008.
Moreno, T., Querol, X., Pey, J., Minguillon, M. C., Perez, N., Alastuey, A., Bernabe, R. M., Blanco, S., Cardenas, B., Eichinger, W., Salcido, A., and Gibbons, W.: Spatial and temporal variations in inhalable CuZnPb aerosols within the Mexico City pollution plume, J. Environ. Monitor., 10, 370–378, doi:10.1039/b716507b, 2008.
Moya, M., Castro, T., Zepeda, M., and Baez, A.: Characterization of size-differentiated inorganic composition of aerosols in Mexico City, Atmos. Environ., 37, 3581–3591, doi:10.1016/s1352-2310(03)00345-5, 2003.
Murphy, D. M.: The design of single particle laser mass spectrometers, Mass Spec. Rev, 26, 150–165, 2007a.
Murphy, D. M., Hudson, P. K., Cziczo, D. J., Gallavardin, S., Froyd, K. D., Johnston, M. V., Middlebrook, A. M., Reinard, M. S., Thomson, D. S., Thornberry, T., and Wexler, A. S.: Distribution of lead in single atmospheric particles, Atmos. Chem. Phys., 7, 3195–3210, 2007b, http://www.atmos-chem-phys.net/7/3195/2007/.
Murphy, D. M., Middlebrook, A. M., and Warshawsky, M.: Cluster analysis of data from the particle analysis by laser mass spectrometry (PALMS) instrument, Aerosol Sci. Technol., 37, 382–391, 2003.
Murphy, D. M. and Thomson, D. S.: Laser ionization mass spectroscopy of single aerosol particles, Aerosol Sci. Technol., 22, 237–249, 1995.
Nash, D. G., Baer, T., and Johnston, M. V. : Aerosol mass spectrometry: An introductory review, Int. J. Mass Spectrom., 258, 2–12, 2006.
Petters, M. D., Prenni, A. J., Kreidenweis, S. M., DeMott, P. J., Matsunaga, A., Lim, Y. B., and Ziemann, P. J.: Chemical aging and the hydrophobic-to-hydrophilic conversion of carbonaceous aerosol, Geophys. Res. Lett., 33, 24, L24806, doi:10.1029/2006gl027249, 2006.
Phares, D. J., Kevin, P. Rhoads, and Wexler, A. S.: Performance of a single ultrafine particle

mass spectrometer, Aerosol Sci. Technol., 36, 583–592, 2002.
Phares, D. J., Rhoads, K. P., Wexler, A. S., Kane, D. B., and Johnston, M. V.: Application of the ART-2a algorithm to laser ablation aerosol mass spectrometry of particle standards, Anal. Chem, 73, 2338–2334, 2001.
Querol, X., Pey, J., Minguillon, M. C., Perez, N., Alastuey, A., Viana, M., Moreno, T., Bernabe, R. M., Blanco, S., Cardenas, B., Vega, E., Sosa, G., Escalona, S., Ruiz, H., and Artinano, B.: PM speciation and sources in Mexico during the MILAGRO-2006 campaign, Atmos. Chem. Phys., 8, 111–128, 2008, http://www.atmos-chem-phys.net/8/111/2008/.
Quinn, P. K. and Bates, T. S.: Regional aerosol properties: Comparisons of boundary layer measurements from ACE 1, ACE 2, aerosols99, INDOEX, ACE asia, TARFOX, and NEAQS, J. Geophys. Res.-Atmos., 110, D14202, doi:10.1029/2004jd004755, 2005.
Ramanathan, V. and Carmichael, G.: Global and regional climate changes due to black carbon, Nature Geoscience, 1, 221–227, 10.1038/ngeo156, 2008.
Sakurai, H., Tobias, H. J., Park, K., Zarling, D., Docherty, S., Kittelson, D. B., McMurry, P. H., and Ziemann, P. J.: On-line measurements of diesel nanoparticle composition and volatility, Atmos. Environ., 37, 1199–1210, doi:10.1016/s1352-2310(02)01017-8, 2003.
Salcedo, D., Onasch, T. B., Dzepina, K., Canagaratna, M. R., Zhang, Q., Huffman, J. A., DeCarlo, P. F., Jayne, J. T., Mortimer, P., Worsnop, D. R., Kolb, C. E., Johnson, K. S., Zuberi, B., Marr, L. C., Volkamer, R., Molina, L. T., Molina, M. J., Cardenas, B., Bernabé, R. M., Màrquez, C., Gaffney, J. S., Marley, N. A., Laskin, A., Shutthanandan, V., Xie, Y., Brune, W., Lesher, R., Shirley, T., and Jimenez, J. L.: Characterization of ambient aerosols in Mexico City during the MCMA-2003 campaign with Aerosol Mass Spectrometry: results from the CENICA Supersite, Atmos. Chem. Phys., 6, 925–946, 2006, http://www.atmos-chem-phys.net/6/925/2006/.
San Martini, F. M., Dunlea, E. J., Grutter, M., Onasch, T. B., Jayne, J. T., Canagaratna, M. R., Worsnop, D. R., Kolb, C. E., Shorter, J. H., Herndon, S. C., Zahniser, M. S., Ortega, J. M., McRae, G. J., Molina, L. T., and Molina, M. J.: Implementation of a Markov Chain Monte Carlo method to inorganic aerosol modeling of observations from the MCMA-2003 campaign – Part I: Model description and application to the La Merced site, Atmos. Chem. Phys., 6, 4867–4888, 2006a, http://www.atmos-chem-phys.net/6/4867/2006/.
San Martini, F. M., Dunlea, E. J., Volkamer, R., Onasch, T. B., Jayne, J. T., Canagaratna, M. R., Worsnop, D. R., Kolb, C. E., Shorter, J. H., Herndon, S. C., Zahniser, M. S., Salcedo, D., Dzepina, K., Jimenez, J. L., Ortega, J. M., Johnson, K. S., McRae, G. J., Molina, L. T., and

Molina, M. J.: Implementation of a Markov Chain Monte Carlo method to inorganic aerosol modeling of observations from the MCMA-2003 campaign – Part II: Model application to the CENICA, Pedregal and Santa Ana sites, Atmos. Chem. Phys., 6, 4889–4904, 2006b, http://www.atmos-chem-phys.net/6/4889/2006/.

Schneider, J., Weimer, S., Drewnick, F., Borrmann, S., Helas, G., Gwaze, P., Schmid, O., Andreae, M. O., and Kirchner, U.: Mass spectrometric analysis and aerodynamic properties of various types of combustion-related aerosol particles, Int. J. Mass Spectrom., 258, 37–49, doi:10.1016/j.ijms.2006.07.008, 2006.

Seinfeld, J. H. and Pandis, S. N.: Atmospheric chemistry and physics: From air pollution to climate change, John Wiley & Sons, Inc., New York, 2006.

Shilling, J. E., King, S. M., Mochida, M., and Martin, S. T.: Mass spectral evidence that small changes in composition caused by oxidative aging processes alter aerosol CCN properties, J. Phys. Chem., 25, 3358–3368, 2007.

Simoneit, B. R. T.: Biomass burning – a review of organic tracers for smoke from incomplete combustion, Appl. Geochem., 17, 129–162, 2002.

Solomon, S., Qin, D., Manning, M., Marquis, M., Averyt, K., Tignor, M., and and Miller, H. L. E.: IPCC: Climate change 2007: The scientific basis, contribution of working group I to the fourth assessment report of the Intergovernmental Panel on Climate Change, Cambridge University Press, Cambridge, United Kingdom and New York, NY, USA, 2007.

Song, X.-H., Hopke, P. K., Fergenson, D. P., and Prather, K. A.: Classification of single particles analyzed by ATOFMS using an artificial neural network, ART-2a, Anal. Chem., 71, 860–865, 1999.

Stockwell, W. R. and Calvert, J. G.: The mechanism of the HO-SO_2 reaction, Atmos. Environ., 17, 2231–2235, 1983.

Stone, E. A., Snyder, D. C., Sheesley, R. J., Sullivan, A. P., Weber, R. J., and Schauer, J. J.: Source apportionment of fine organic aerosol in Mexico City during the MILAGRO experiment 2006, Atmos. Chem. Phys., 8, 1249–1259, 2008, http://www.atmos-chem-phys.net/8/1249/2008/.

Su, Y., Sipin, M. F., Furutani, H., and Prather, K. A.: Development and characterization of an aerosol time-of-flight mass spectrometer with increased detection efficiency, Anal. Chem., 76, 712–719, 2004.

Sullivan, R. C. and Prather, K. A.: Recent advances in our understanding of atmospheric chemistry and climate made possible by on-line aerosol analysis instrumentation, Anal. Chem, 77,

3861–3886, 2005.
Sun, J. M. and Ariya, P. A.: Atmospheric organic and bio-aerosol as cloud condensation nuclei (CCN): A review, Atmos. Environ., 40, 795–820, 2006.
Takegawa, N., Miyazaki, Y., Kondo, Y., Komazaki, Y., Miyakawa, T., Jimenez, J. L., Jayne, J. T., Worsnop, D. R., Allan, J. D., and Weber, R. J.: Characterization of an Aerodyne Aerosol Mass Spectrometer (AMS): Intercomparison with other aerosol instruments, Aerosol Sci. Technol., 39, 760–770, 2005.
Tanaka, P. L., Riemer, D. D., Chang, S., Yarwood, G., McDonald Buller, E. C., Apel, E. C., Orlando, J. J., Silva, P. J., Jimenez, J. L., Canagaratna, M. R., Neece, J. D., Mullins, C. B., and Allen, D. T.: Direct evidence for chlorine-enhanced urban ozone formation in Houston, Texas, Atmos. Environ., 37, 1393–1400, 2003.
Thomson, D. S., Schein, M. E., and Murphy, D. M.: Particle analysis by laser mass spectrometry WB 57F instrument overview, Aerosol Sci. Technol., 33, 153–169, 2000.
Ulbrich, I. M., Canagaratna, M. R., Zhang, Q., Worsnop, D. R., and Jimenez, J. L.: Interpretation of organic components from positive matrix factorization of aerosol mass spectrometric data, Atmos. Chem. Phys. Discuss., 8, 6729–6791, 2008, http://www.atmos-chem-phys-discuss.net/8/6729/2008/.
Volkamer, R., Jimenez, J. L., San Martini, F., Dzepina, K., Zhang, Q., Salcedo, D., Molina, L. T., Worsnop, D. R., and Molina, M. J.: Secondary organic aerosol formation from anthropogenic air pollution: Rapid and higher than expected, Geophys. Res. Lett., 33, 17, L17811, doi:10.1029/2006gl026899, 2006.
Yokelson, R. J., Urbanski, S. P., Atlas, E. L., Toohey, D. W., Alvarado, E. C., Crounse, J. D., Wennberg, P. O., Fisher, M. E., Wold, C. E., Campos, T. L., Adachi, K., Buseck, P. R., and Hao, W. M.: Emissions from forest fires near Mexico City, Atmos. Chem. Phys., 7, 5569–5584, 2007, http://www.atmos-chem-phys.net/7/5569/2007/.
Zelenyuk, A. and Imre, D.: Single particle laser ablation time-of-flight mass spectrometer: An introduction to SPLAT, Aerosol Sci. Technol., 39, 554–568, doi:10.1080/027868291009242, 2005.
Zhang, Q., Jimenez, J. L., Canagaratna, M. R., Allan, J. D., Coe, H., Ulbrich, I., Alfarra, M. R., Takami, A., Middlebrook, A. M., Sun, Y. L., Dzepina, K., Dunlea, E., Docherty, K., DeCarlo, P. F., Salcedo, D., Onasch, T., Jayne, J. T., Miyoshi, T., Shimono, A., Hatakeyama, S., Takegawa, N., Kondo, Y., Schneider, J., Drewnick, F., Weimer, S., Demerjian, K., Williams, P., Bower, K., Bahreini, R., Cottrell, L., Griffin, R. J., Rautiainen, J.,

and Worsnop, D. R.: Ubiquity and dominance of oxygenated species in organic aerosols in anthropogenically–influenced northern hemisphere mid-latitudes, Geophys. Res. Lett., 34, 13, L13801, doi:10.1029/2007gl029979, 2007.

Zhang, Q., Canagaratna, M. R., Jayne, J. T., Worsnop, D. R., and Jimenez, J.-L.: Time- and size-resolved chemical composition of submicron particles in Pittsburgh: Implications for aerosol sources and processes, J. Geophys. Res., 110, D7, D07s09, doi:10.1029/2004jd004649, 2005a.

Zhang, Q., Alfarra, M. R., Worsnop, D. R., Allan, J. D., Coe, H., Canagaratna, M. R., and Jimenez, J. L.: Deconvolution and quantification of hydrocarbon-like and oxygenated organic aerosols based on aerosol mass spectrometry, Environ. Sci. Technol., 39, 4938–4952, 2005b.

Zhang, Q., Worsnop, D. R., Canagaratna, M. R., and Jimenez, J. L.: Hydrocarbon-like and oxygenated organic aerosols in Pittsburgh: Insights into sources and processes of organic aerosols, Atmos. Chem. Phys., 5, 3289–3311, 2005c, http://www.atmos-chem-phys.net/5/3289/2005/.

Zhang, X., Smith, K. A., Worsnop, D. R., Jimenez, J. L., Jayne, J. T., Kolb, C. E., Morris, J., and Davidovits, P.: Numerical characterization of particle beam collimation: Part II integrated aerodynamic lens-nozzle system, Aerosol Sci. Technol., 38, 619–638, 2004.

Table 1. Single particle properties of two externally mixed particles shown in Fig. 7.

Particle Property	Velocity (m/s)	d_{va} (nm)	d_o (nm)	Total Mass Measured by Mass Spectrometer (fg)	Chemical Physical Diameter (nm)	Optical Density (g/cm^3)	Predicted Density (g/cm^3)	Calculated Total Mass (fg)
Particle #1	106	287	301	18.2	0.9	0.95	326	13.64
Particle #2	94	446	263	13.0	1.48	1.70	211	16.14

ACPD
8, 21313–21381, 2008

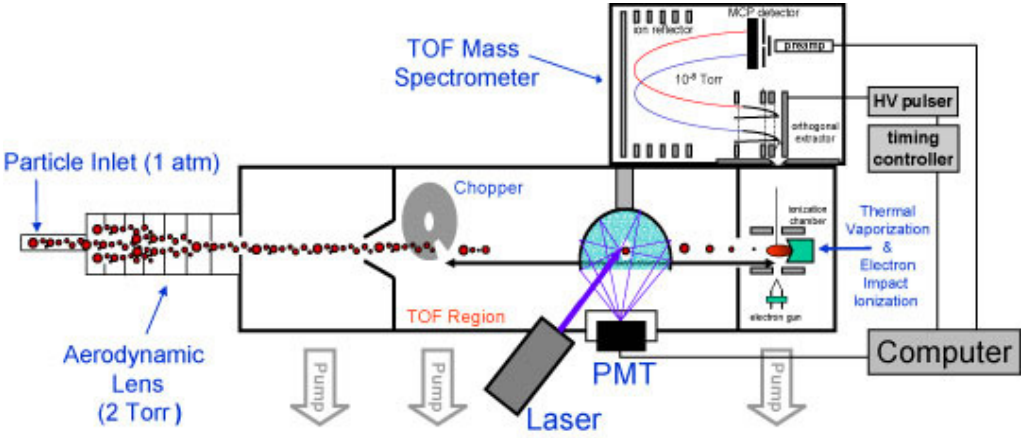

Fig. 1. Schematic of the LS-ToF-AMS.

ACPD
8, 21313–21381, 2008

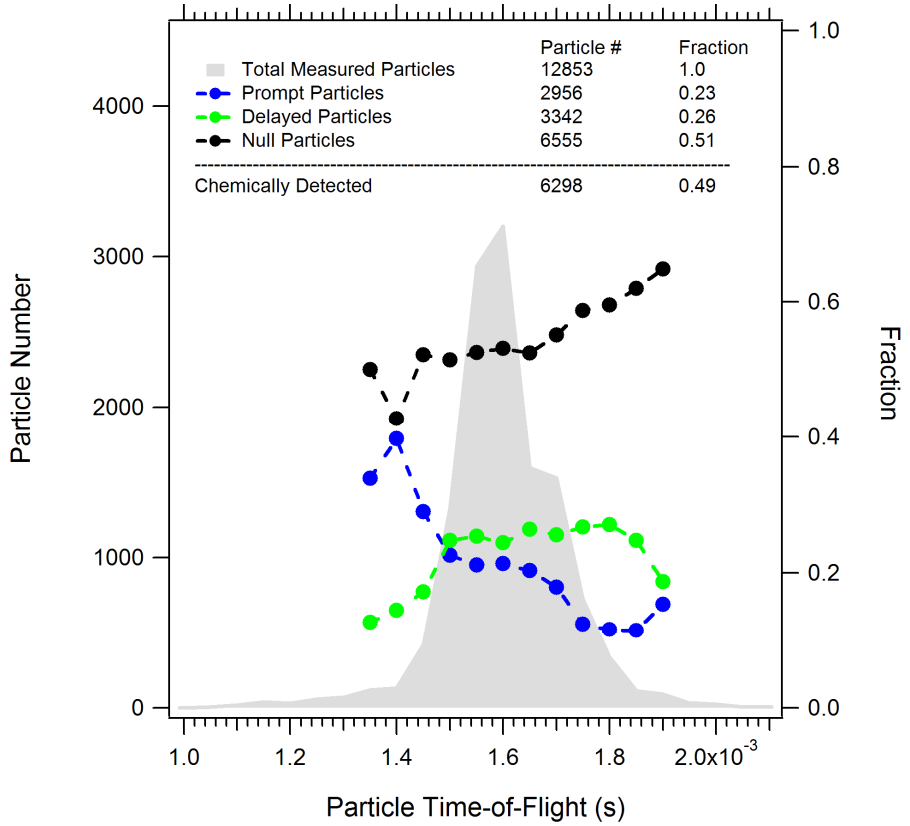

Fig. 2. Total particle counts (in grey) and number fractions of prompt (blue), delayed (green) and null (black) particles as a function of time-of-flight (i.e. d_{va}).

ACPD
8, 21313–21381, 2008

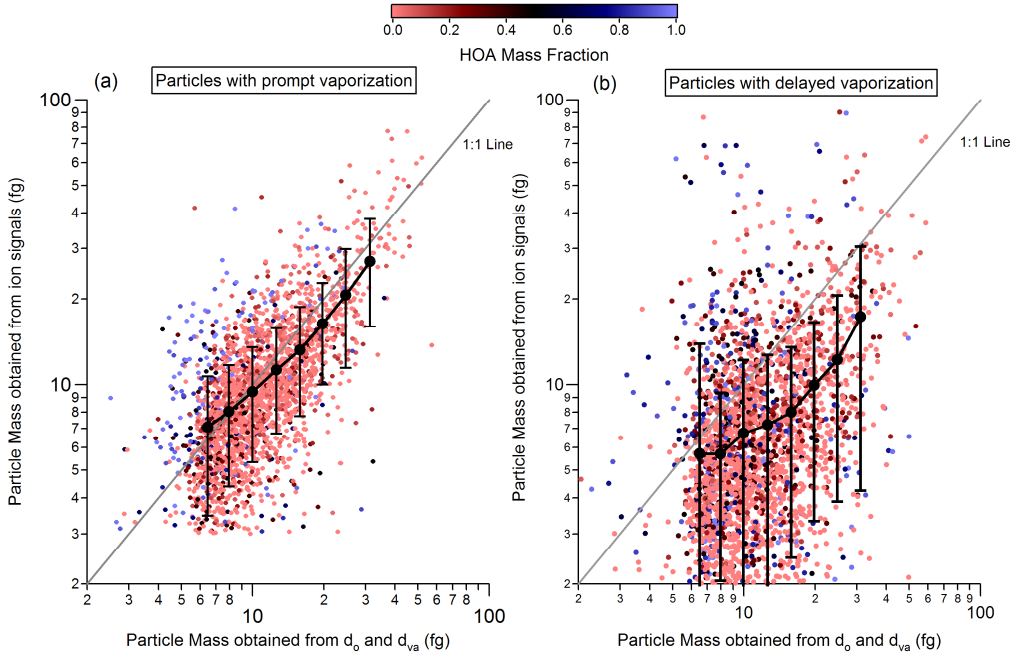

Fig. 3. Measured single particle mass obtained from chemical ion signals plotted versus single particle mass obtained from optical diameter (d_o) and vacuum aerodynamic diameter (d_{va}) measurements for **(a)** particles with prompt vaporization and **(b)** particles with delayed vaporization.

ACPD
8, 21313–21381, 2008

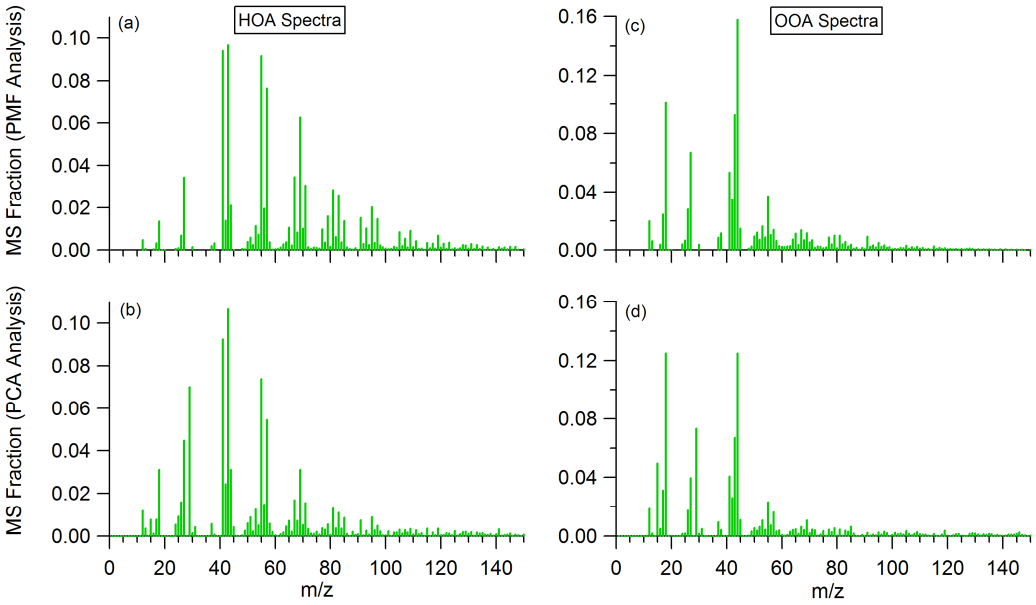

Fig. 4. Average HOA and OOA organic mass spectra obtained from ambient ensemble measurements using PMF analysis (upper region, plots **a** and **c**) and two-component PCA analysis (lower region plots **b** and **d**).

ACPD
8, 21313–21381, 2008

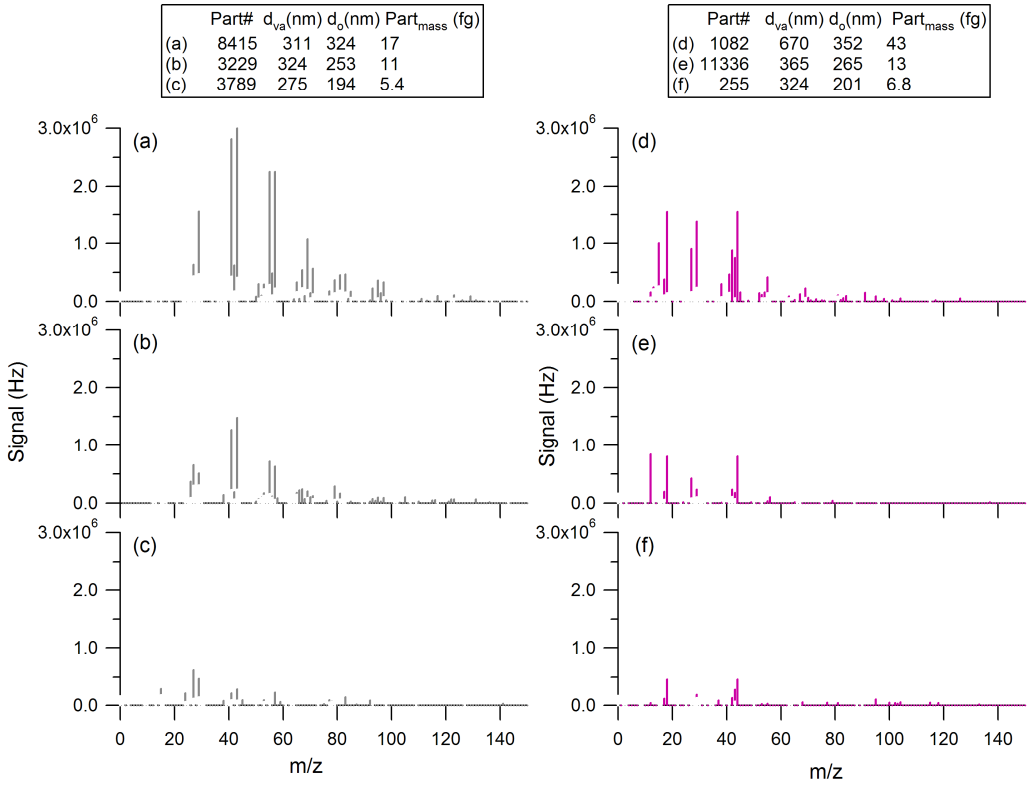

Fig. 5. Six single particle mass spectra obtained for three different sized organic particles (d_o~ 200, 250, and 350 nm) predominately composed of HOA **(a–c)** and OOA **(d–f)** components. Particle d_{va}, d_o, and mass are shown in the insert.

ACPD
8, 21313–21381, 2008

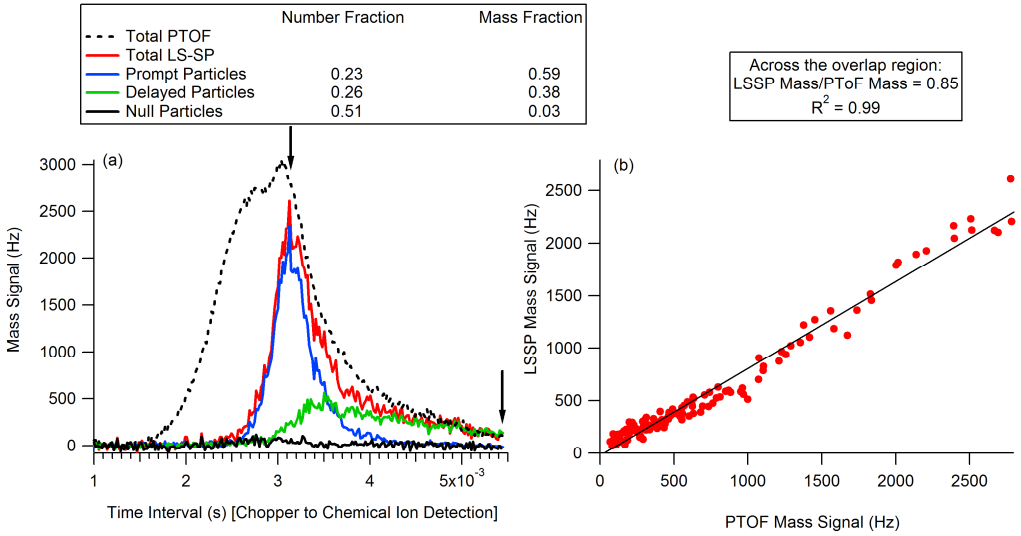

Fig. 6. (a) Average mass distributions as a function of particle time-of-flight for ensemble data (dashed black line) and total single particle data (red line). Distributions for prompt (blue), delayed (green) and null (black) particles are also shown. **(b)** Correlation plot between the average PToF and total single particle mass measurements for times-of-flight between 3.1–5.5 ms, denoted with arrows in (a).

ACPD
8, 21313–21381, 2008

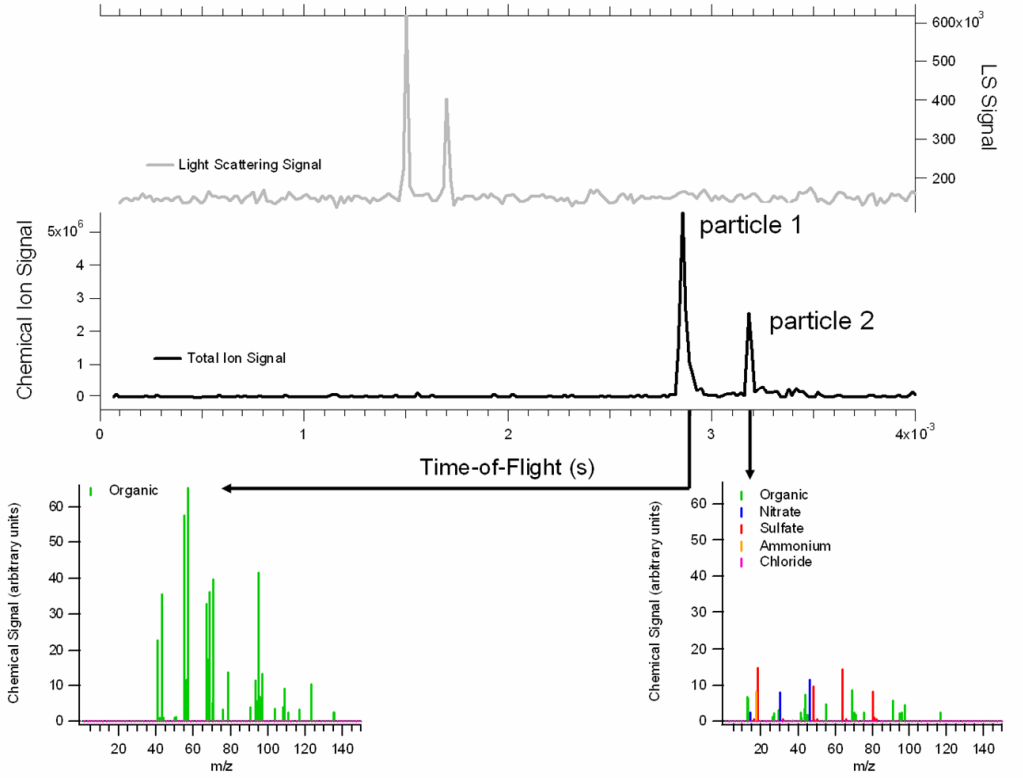

Fig. 7. Light scattering signals (upper panel) and chemical ion signals (middle panel) as a function of particle time-of-flight for a single chopper cycle in which two particles entered the LS-ToF-AMS. The lower panel displays the mass spectrum of each particle.

ACPD
8, 21313–21381, 2008

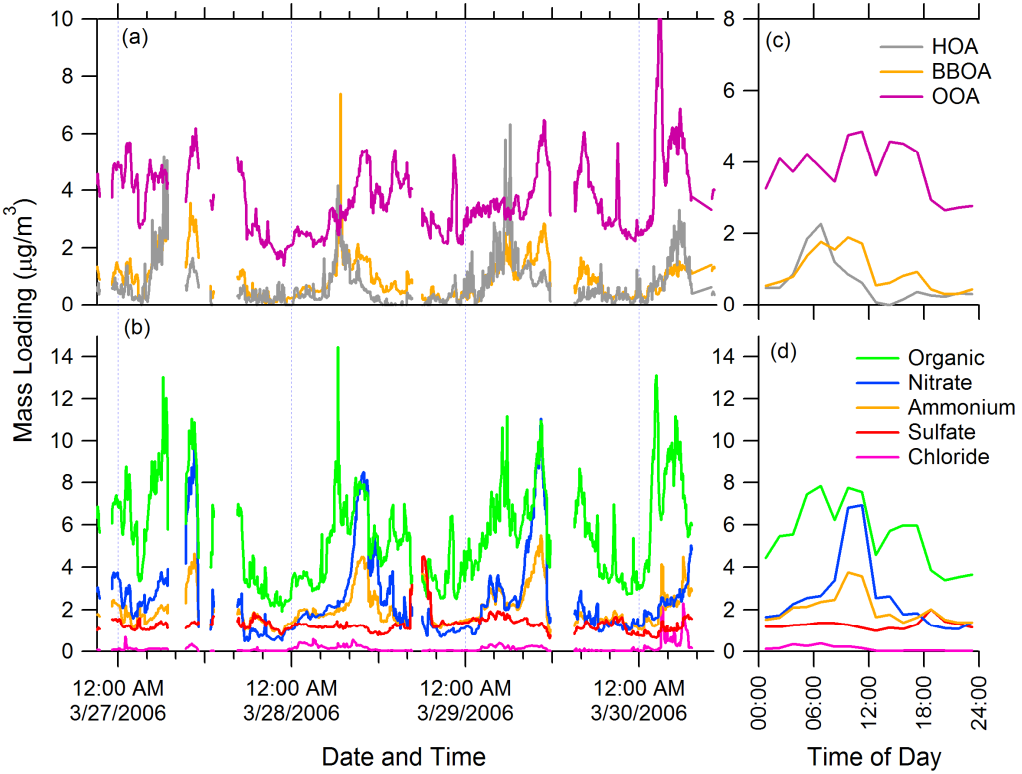

Fig. 8. Average ensemble mass concentrations (measured in MS mode) as a function of sampling time. **(a)** Organic components obtained from PMF analysis – OOA, BBOA, and HOA. **(b)** Chemical components obtained from traditional AMS fragmentation patterns – organic, nitrate, sulfate, ammonium, and chloride. Average diurnal cycles, for the full 75 sampling period, of each chemical component are displayed in plots **(c)** and **(d)**.

ACPD
8, 21313–21381, 2008

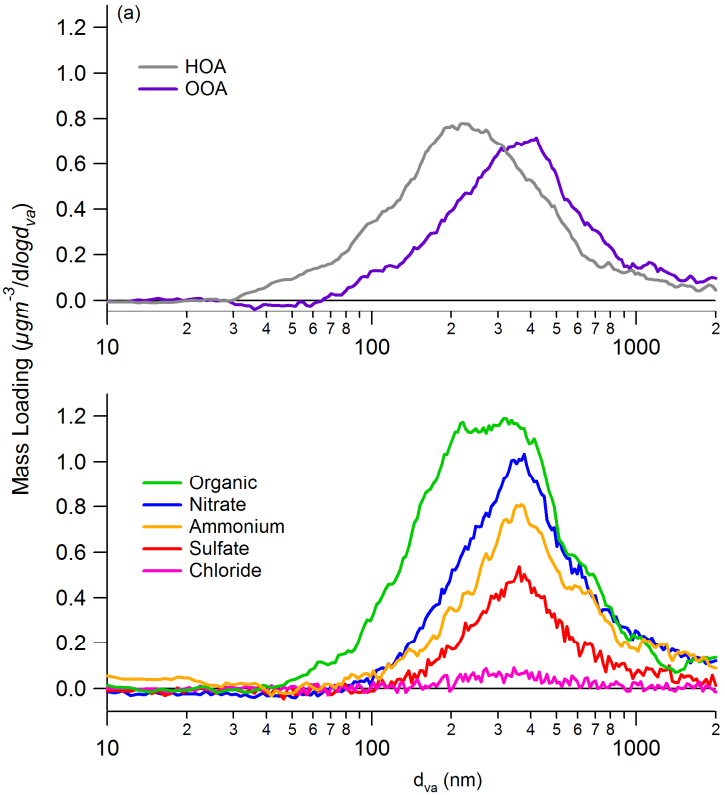

Fig. 9. Average ensemble mass distributions (measured in PTOF mode) as a function of vacuum aerodynamic diameter (d_{va}) for **(a)** HOA and OOA components and **(b)** organic, nitrate, sulfate, ammonium, and chloride.

ACPD
8, 21313–21381, 2008

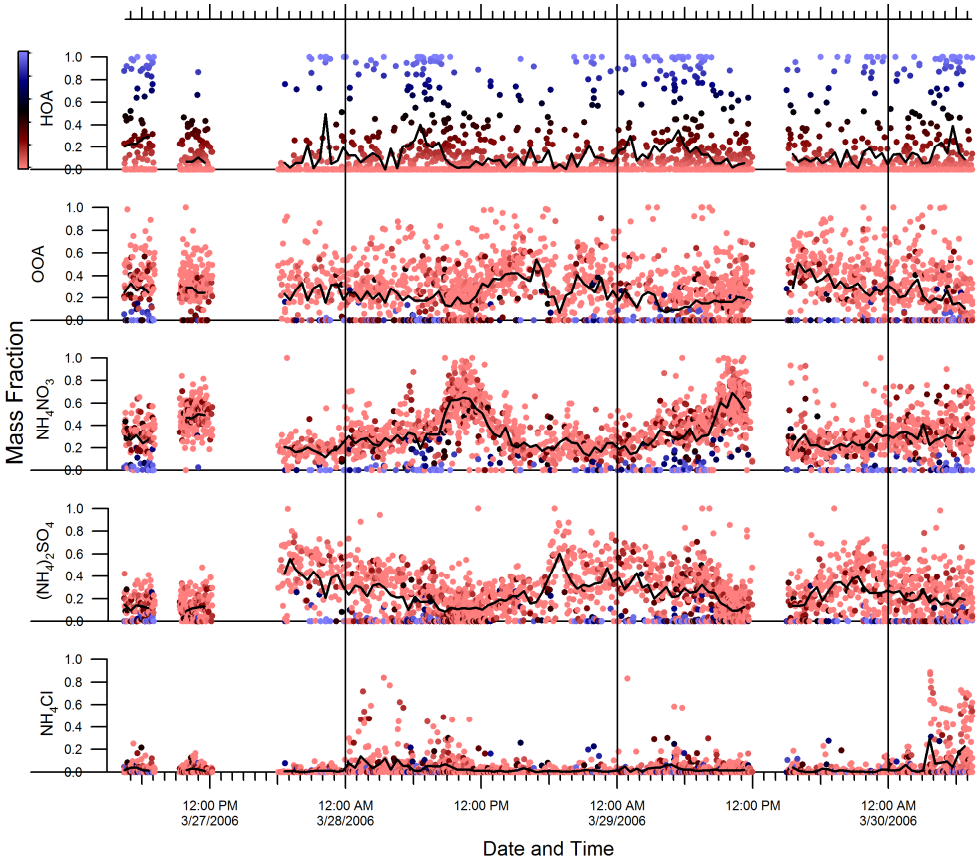

Fig. 10. Time series of NH_4Cl, $(NH_4)_2SO_4$, NH_4NO_3, OOA, and HOA single particle mass fractions. Data points are colored by HOA mass fraction as indicated in the upper left.

ACPD
8, 21313–21381, 2008

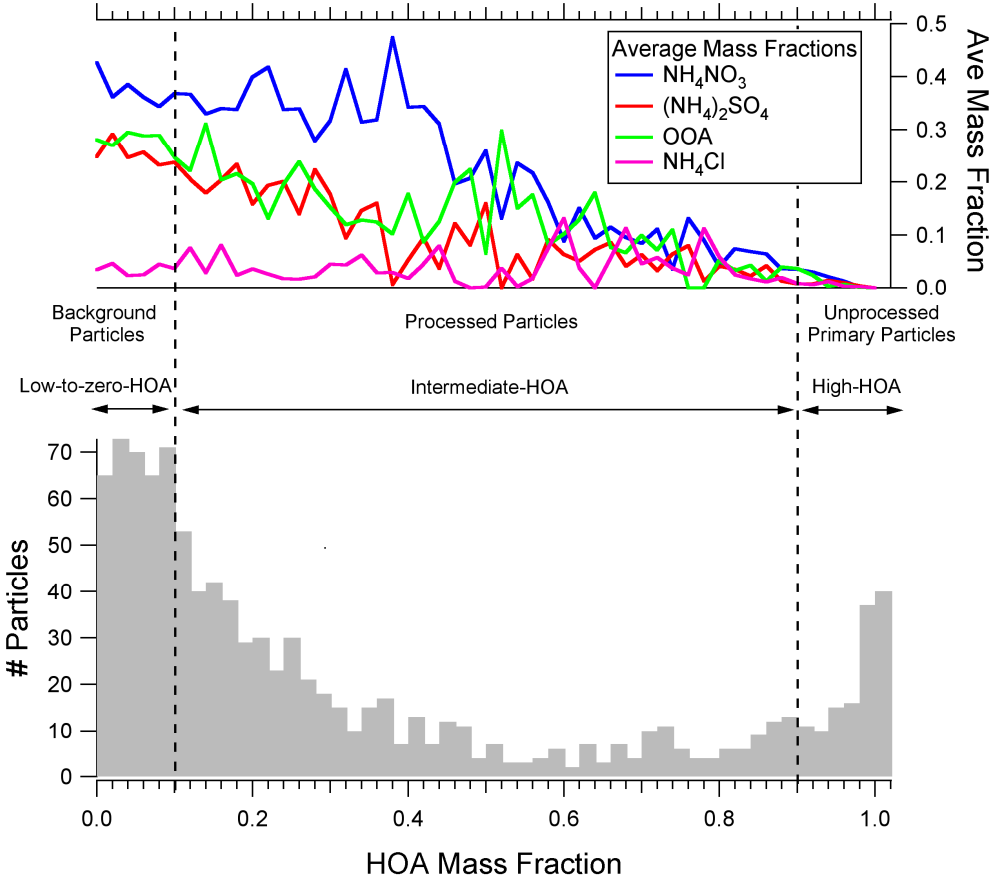

Fig. 11. Particle counts (lower panel) and average single particle composition (upper panel) as a function of HOA mass fraction.

ACPD
8, 21313–21381, 2008

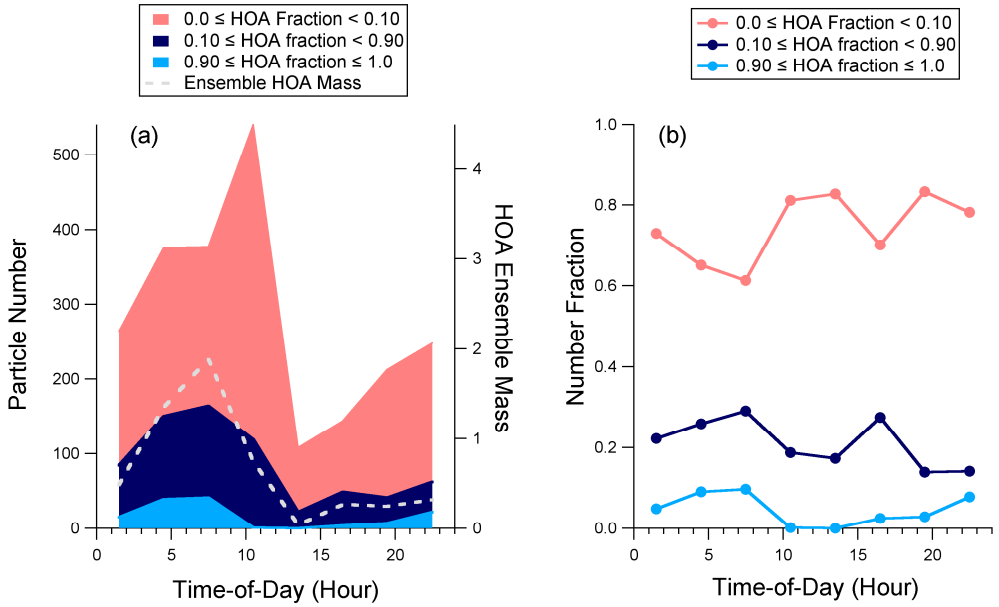

Fig. 12. Time trends in the **(a)** measured number and **(b)** number fraction of high-HOA, intermediate-HOA, and low-to-zero-HOA particles.

ACPD
8, 21313–21381, 2008

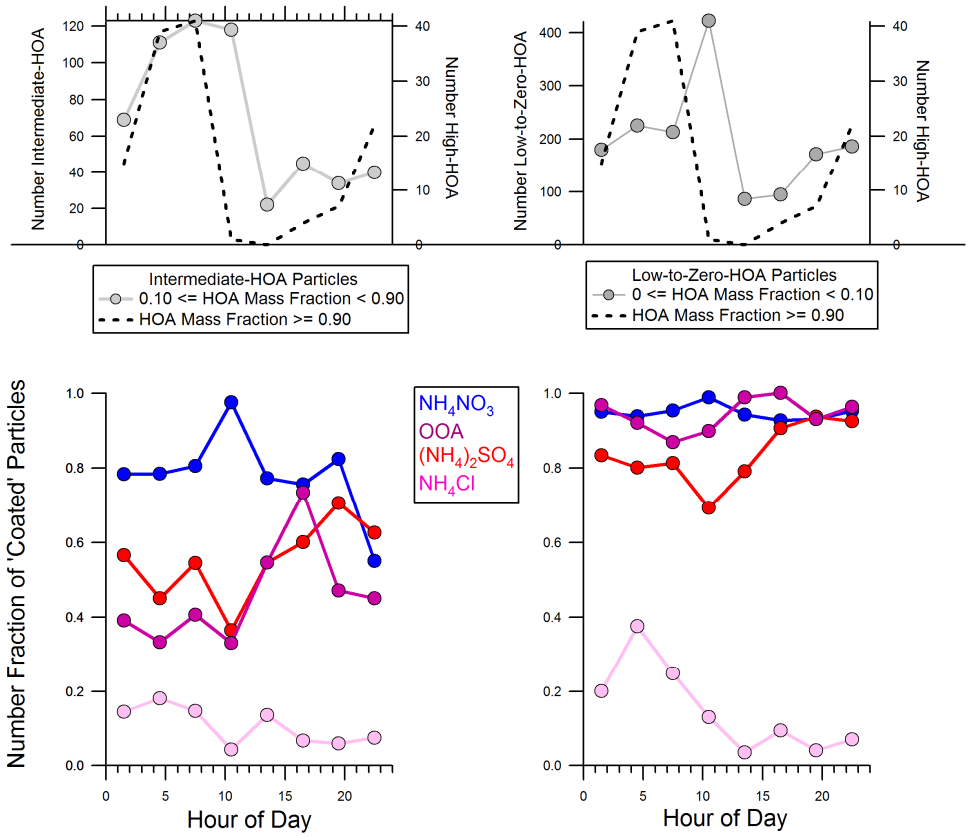

Fig. 13. Time trends in the number (upper panel) and number fraction of "coated" particles for **(a)** intermediate-HOA particles and **(b)** low-to-zero-HOA particles.

ACPD
8, 21313–21381, 2008

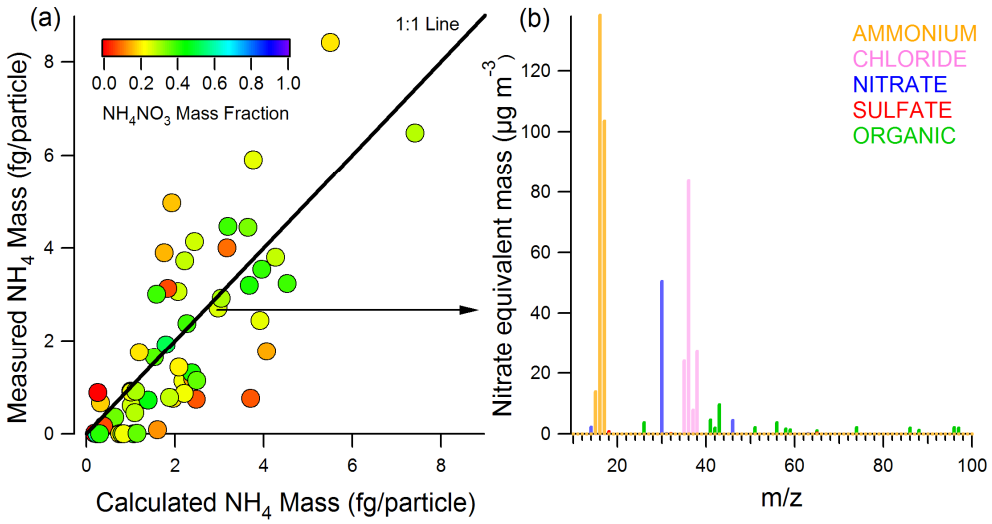

Fig. 14. **(a)** Measured (i.e. real) single particle NH_4 mass plotted versus calculated single particle NH_4 mass for the subset of single particles with high chloride content. **(b)** Single particle mass spectrum for a typical high chloride content particle (identified in (a) with the arrow).

ACPD
8, 21313–21381, 2008